8-2010

Synthesis and characterization of ceria nanomaterials.

Nitzia Cheong Ng
University of Louisville

Recommended Citation

Ng, Nitzia Cheong, "Synthesis and characterization of ceria nanomaterials." (2010). *Electronic Theses and Dissertations.* Paper 1054.
https://doi.org/10.18297/etd/1054

SYNTHESIS AND CHARACTERIZATION OF CERIA NANOMATERIALS

By

Nitzia Cheong Ng
B.S., University of Louisville, May 2009

A Thesis
Submitted to the Faculty of the
University of Louisville
J. B. Speed School of Engineering
as Partial Fulfillment of the Requirements
for the Professional Degree

MASTER OF ENGINEERING

Department of Chemical Engineering

August 2010

SYNTHESIS AND CHARACTERIZATION OF CERIA NANOMATERIALS

Submitted by: ___________________________________
Nitzia Cheong Ng

A Thesis Approved On

____
Date

by the Following Reading and Examination Committee:

____
Dr. Xiao-An Fu, Thesis Advisor

____
Dr. James C. Watters

____
Dr. Gamini Sumanasekera

ACKNOWLEDGEMENTS

The author is grateful for the support, knowledge, and patience of Dr. Xiao-An Fu, Thesis Advisor.

The author thanks Jacek Jasinski and Rodica McCoy for their help in characterization.

The author appreciates Dr. James Watters for participating in the defense committee.

The author appreciates Dr. Gamini Sumanasekera for participating in the defense committee.

The author also thanks Surender Venna, Chinmay Deshmane and Dr. Moises Carreon for their help and knowledge in BET and Dr. Kyung Kang and Dr. Martin O’Toole for the centrifugation instrument.

The author is gratified to Dr. Michael Tseng from the Medical School for his knowledge and support.

ABSTRACT

Cerium dioxide or ceria, $CeO_{2,}$ has been widely used in industry as catalyst for automotive exhaust controls, chemical mechanical polishing (CMP) slurries, and high temperature fuel cells because of its unique metal oxide properties. This well-known rare metal oxide has high thermal stability, electrical conductivity and chemical diffusivity. Proper synthesis method requires knowledge of reaction temperature, concentration, and time effects on the synthesis. In this work, ceria nanomaterials were prepared via the hydrothermal method using a Teflon autoclave. Cerium nitrate solution was used as the source and three different precursors: NaOH, H_2O_2, and NH_4OH were used as the oxidizing agents. CeO_2 nanoplates, nanocubes and nanorods were produced and studied using transmission electron microscopy (TEM), BET specific surface area, X-ray diffraction (XRD) and X-ray photoelectron spectroscopy (XPS).

Through characterization, CeO_2 nanomaterials showed the presence of mixed valence states (Ce^{3+} and Ce^{4+}) through XPS spectra. Deconvolution was performed to investigate the ratio of Ce^{3+}/Ce^{4+} concentration in the synthesized CeO_2 nanostructures. Nanocubes showed a higher Ce^{3+} concentration. CeO_2 nanomaterials were found to be mesoporous. Nanoplates synthesized with H_2O_2, and NH_4OH were found with surface areas of 95.11 m^2/ g and 62.07 m^2/ g, respectively. Nanorods and nanocubes showed surface areas of 16.77 m^2/ g and 16.55 m^2/ g, respectively. The prepared ceria nanoplates, nanocubes and nanorods had crystallite size in the range of 5-25 nm and pore size range of 7-15 nm. XRD spectra confirmed that the peaks were indexed to the cubic phase of

CeO_2 with fluorite structure and with an average lattice parameter, 5.407 Å. Higher Ce^{3+} concentration and exposed surface of crystalline planes suggest that nanorods are better catalyst for CO oxidation and oxygen storage capacity (OSC).

TABLE OF CONTENTS

NOMENCLATURE

NH_4OH = Ammonium hydroxide

BE = Binding energy

BJH = Barret-Joyner-Halenda

BET = Brunaure Emmett Teller

CO = Carbon dioxide oxidation

CeO_2 = Ceria or cerium oxide

$Ce(NO_3)_3$ = Cerium nitrate

C_{NaOH} = Concentration of sodium hydroxide

d_{hkl} = Crystalline face space at the crystallite indices

D_{hkl} = Crystallite size at the crystallite indices

h,k,l = Crystallite size indices

TG-DTA = Differential thermal analysis and thermo-gravimetric analysis

θ = Diffraction angle

FCC = Face –centered-cubic

FFT = Fast Fourier transform

FT-IR = Fourier transform infrared

H_2O_2 = Hydrogen peroxide

HRTEM = High-resolution transmission electron microscopy

n = Integer number, usually 1

A_i = Integrated area of peak “*i*.”

a = Lattice parameter

B_{hkl} = Measured half-width

OSC = Oxygen storage capacity

SAED = Selected area electron diffraction

NaOH = Sodium hydroxide

H_2- TPR = Temperature-programmed reduction of hydrogen

TEM = Transmission electron microsope

λ = Wavelength of the incident X-rays

XPS = X-ray photoelectron spectroscopy

XRD = X-ray diffraction

LIST OF TABLES

LIST OF FIGURES

I. INTRODUCTION

Studies in the morphologies and sizes of cerium dioxide or ceria have attracted the interests of researchers in recent years due to ceria’s unique properties that lead to a wide range of applications. Some examples of ceria applications include fast ion conductors, UV blockers, catalyst (Tang, 2005), gas and bio-sensors, cosmetic material, fuel cells, and slurry for chemical mechanical planarization (Seok, 2004). Several synthetic approaches such as electrochemical deposition, microwave-hydrothermal, solvothermal, hydrothermal and others have been developed to form ceria nanomaterials. Of these methods, the hydrothermal method (Mai, 2005) has been considered as one of the most effective and economical routes, because of its single step low-temperature synthesis, superior composition and morphological control, and powder reactivity.

To explore the morphology and properties of ceria, proper synthesis and precursors are required to obtain specific ceria nanostructures. The present work investigates the different shapes of ceria formed by using three different precursors: hydrogen peroxide, ammonium hydroxide, and sodium hydroxide through hydrothermal method for 24 hours. The different precursors and reaction parameters such as time, temperature, and concentration influence the size and shape of ceria, forming nanoplates, nanorods, and nanocubes.

In the current project, ceria is synthesized from cerium nitrate and three different precursors mentioned earlier. Once the synthesis was done, the samples were centrifuged, purified by washing several times, and dried. The dried precipitates show the following colors: white for the synthesis with H_2O_2, light yellow with NaOH, and medium yellow with NH_4OH. Characterization is performed to understand the morphologies and properties of ceria formed using each precursor. In this work, the samples have been characterized with TEM, X-Ray diffraction, BET specific surface area, and XPS to understand their properties.

II. BACKGROUND

A. Cerium Oxide or Ceria

Cerium with an atomic number 58 has brought new discoveries in terms of nanomaterials. Cerium is the most abundant of the rare earth elements. As a well-known functional rare earth material, ceria has wide applications in fields such as catalysis, electrochemistry, and optics due to its unique properties (Powell, 1988). In addition, cerium dioxide has been extensively studied and employed in various applications including fast ion conductors, oxygen storage capacitors, catalysts, UV blockers, polishing materials (Tang, 2005), and gas sensor (Yahiro, 1988).

Preparation of ceria powders is by no means a new research subject; however, practical methods are still needed for synthesizing high-quality ultrafine powders with required characteristics in terms of their size, uniformity, morphology, specific surface area, and crystallinity. Numerous techniques have been proposed to synthesize nano-sized CeO_2 particles with promising control of properties (Lee, 2004; Zhou, 1995).

Cerium dioxide has been used in many catalysis applications. Trovarelli (1996 and 2002) reported that CeO_2 has been extensively studied and applied in heterogeneous catalysis based on its ability to release and uptake oxygen under operation conditions while preserving the fluorite crystal structure. It has an important role in two of the most important commercial catalytic processes in terms of economic relevance and tonnage: three-way catalysis (TWC) and fluid catalytic cracking (FCC). The importance of CeO_2 in catalysis is also exhibited by the number of industrial and academic publications that have appeared on the topic over the last several years as shown in Figure 2.1. In 1997, the number of published ceria topics reveals that approximately 50% is based on the treatment of emissions from mobile and stationary sources, and that the majority of articles deal with the application of ceria in TWCs and novel technologies for the treatment of emissions from diesel and spark-ignited internal combustion engines as shown in Figure 2.2 (Trovarelli, 1999).

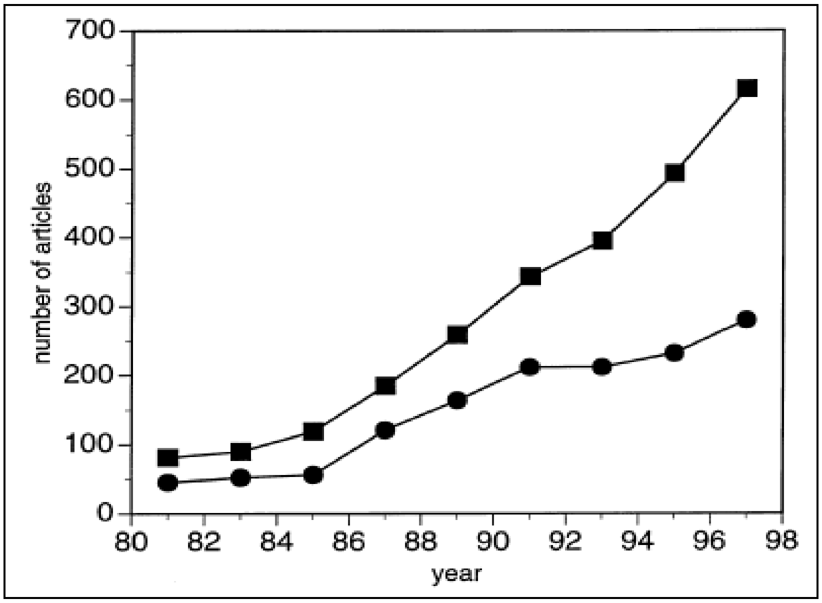

FIGURE 2.1 - Number of publications on CeO2-based materials in catalysis: (■) open literature, (●) patents (Trovarelli, 1999).

This indicates that there are several rising applications or processes for which cerium oxide is currently being actively investigated. Trovarelli mentioned that ceria acts as an oxygen buffer by absorbing and releasing oxygen through a fast Ce^{3+}/Ce^{4+} cycle in the TWCs, and simultaneously encouraging the oxidation of CO to CO_2 and involving the participation of the lattice oxygen species.

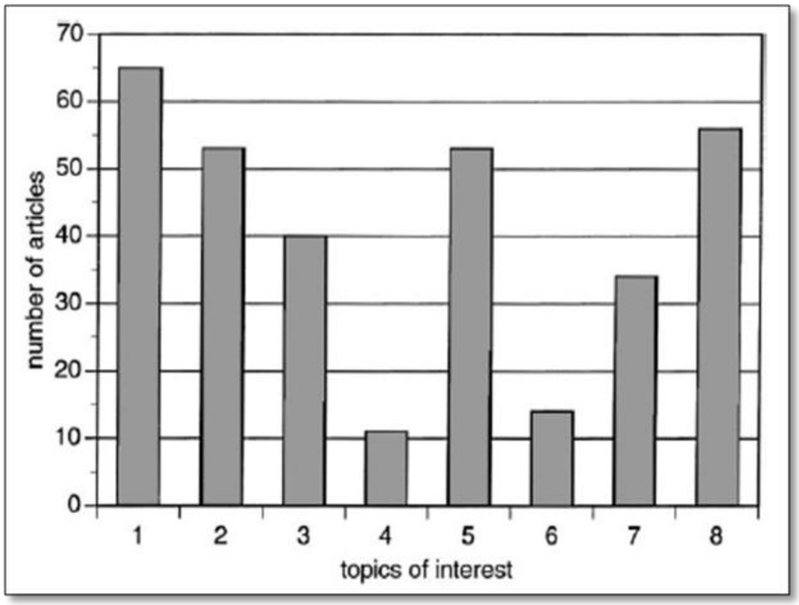

FIGURE 2.2- Number of scientific articles (not patents) published in 1997 on ceria and related materials in different areas of catalysis: 1 (TWC), 2 (flue gas treatment), 3 (oxidation), 4 (treatment of diesel exhaust), 5 (catalyst characterization), 6 (electrocatalysis), 7 (hydrogenation), 8 (others) (Trovarelli, 1999).

Additionally, the unique redox property is usually described by the oxygen storage capacity (OSC), which is largely dependent on the size of ceria particles (Carrettin, 2004; Trovarelli, 1996 and 2002). The morphology also contributes to the redox feature of ceria depending on the exposed ceria crystalline planes (Mai; 2005; Zhou, 2005). Lastly, it was found that CeO_2 has potential uses (Trovarelli, 1996) as diesel fuels catalyst for a more complete combustion to abate soot formation, and for higher-energy efficiency and energy density of solid-oxide fuel-cell.

B. Hydrogen Peroxide

The preparation of ceria using hydrogen peroxide as an oxidizer has been a facile method through hydrothermal synthesis. Several methods have been used to synthesize ceria nanowires by cerium nitrate ($Ce(NO_3)_3$) with H_2O_2. For example, Figure 2.3 shows a TEM image of CeO_2 nanowires by hydrothermal method. The obtained CeO_2 nanowires are single crystalline and uniform with diameters of 20-70 nm and lengths up to 40 μm (Tang, 2005).

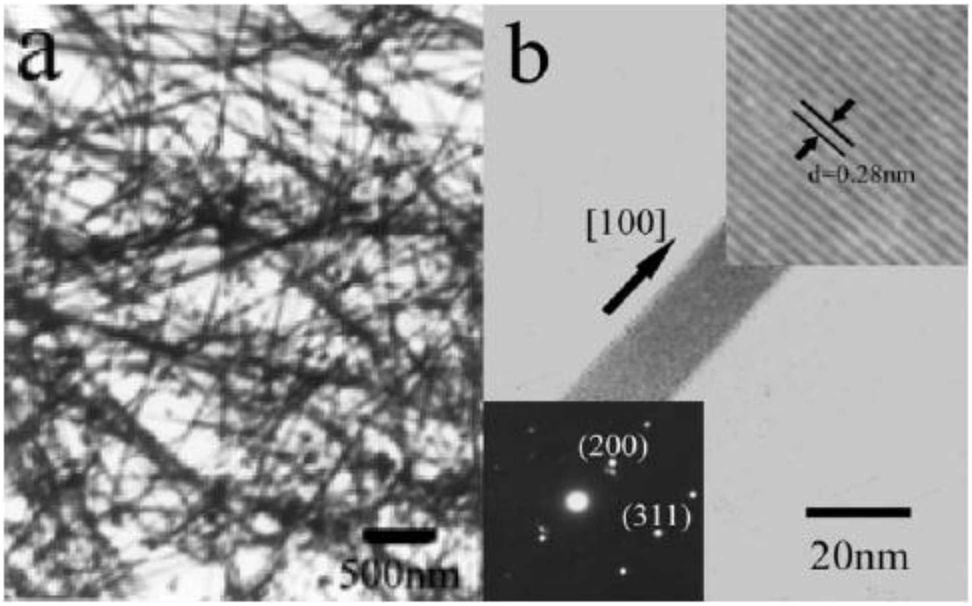

FIGURE 2. 3 - a) TEM image of CeO_2 nanowires, b) HRTEM image of individual CeO_2 nanowire (Tang,2005).

On the other hand, H_2O_2 with cerium nitrate can form CeO_2 nanoplates as described in Chapter IV. The morphology (Mai, 2005; Zhou, 2005) is mainly composed of polyhedron which exposes eight {1 1 1} or eight {1 1 1} and six {1 0 0} plane, but the rod-shaped nanostructures tend to preferentially expose four {1 1 0} and two {1 0 0} planes. Therefore, Mai et al. (2005) reported that the oxygen storage is confined mainly on the surface of CeO_2 nanoparticles, while the oxygen species both on the surface and in the bulk could participate in the redox cycle in the nanorods, giving a much higher OSC (Mai, 2005). Djuricic et al. (1999) reported that the role of H_2O_2 is to make it much easier to change the valence state of cerium ion from Ce (III) to Ce (IV). The following reaction takes place in solution:

$$Ce^{3+} + H_2O_2 + 2H^{+} \text{ (aq.)} \rightarrow Ce^{4+} + 2H_2O$$

To obtain cerium(IV) oxide from Ce(III) nitrate, H_2O_2 is used as an oxidizer, owing to the H-bond interaction with other hydroxyl or hydroperoxyl groups at two-directions. Tang et al. (2005) revealed that H_2O_2 was also a template agent. In contrast with most of the other templates, which can generate complicated process and an increase of impurity concentration in the final product, H_2O_2 makes the process very simple and does not leave any impurity in the hydrothermal reaction system. The H_2O_2-assisted hydrothermal method might offer an opportunity to synthesize other similar nanomaterials and have significant contribution for industrial applications. CeO_2 nanoparticles have significant impact in applications such as UV blocking and shielding materials. This is because of their considerably small sizes, high surface areas, and especially the general improvements in the material properties with respect to their micronized or bulk like materials (Mai, 2005).

C. Ammonium Hydroxide

Ceria nanoplates are also formed by using the second precursor ammonium hydroxide. Recently, nanoplates have attracted increasing attention due to two advantages: one is high crystallinity and well-defined chemical composition as well as extremely high anisotropy with an ultrathin thickness (Zhang, 2005) and the other is that they are superior precursors to be used for conversion into other nanostructrures (Tian, 2002), such as nanotubes based on the rolling-up mechanism. Therefore, CeO_2 nanoplates are hoped to be synthesized so that they can improve the catalytic performance and also be easy to convert into other useful nanostructures.

Besides producing CeO_2 nanoplates, other approaches have successfully formed CeO_2 nanoparticles by adding aqueous ammonium hydroxide precipitant into cerium nitrate solution at room temperature and introducing oxygen into the reactor to oxidize Ce^{3+} to $Ce4^{+}$ (Zhou, 2002). Han et al (2005) proved that CeO_2 nanowires with a diameter range from 5-30 nm and a length up to several microns shown in Figure 2.4 can be formed by adding aqueous ammonium hydroxide precipitant into cerium nitrate at 70°C and then aging at 0 °C for 1 day. Chen et al. (2004) reported that high-alkaline environments support the oxidation of $Ce(OH)_3$ to hydrated Ce (IV). Oxidation of Ce^{3+} to Ce^{4+} in solution takes place at high pH, for example, $Ce^{3+} + H_2O \rightarrow Ce\,(OH)^{3+} + H^+ + e^-$ with subsequent hydrolysis to $Ce(OH)_4$ and precipitation. Hydroxyl ions play an important role in this process and strongly affect the upper saturation degree of initial precipitate and oxidation of Ce (III) to Ce (IV).

FIGURE 2.4 – HRTEM image of CeO_2 nanowires (Han, 2005).

An enhanced catalytic activity was found for CO oxidation by using CeO_2 nanoplates as compared with CeO_2 nanotubes and nanorods, and the crystal surfaces (100) of CeO_2 nanoplates were considered to play an important role in determining their catalytic oxidation properties. The structural characteristics of CeO_2 are believed to affect their performance in catalysis and can be extended to other technological applications (Pan, 2008).

D. Sodium Hydroxide

In order to achieve ceria nanorods and nanocubes, sodium hydroxide precursor helps to obtain these morphologies. Cerium nitrate is synthesized with sodium hydroxide to form different crystal structures, shapes and sizes. Table I presents the synthesis factors used to obtain these types of CeO_2 morphologies. Mai et al. (2005) found that CeO_2 nanorods and nanocubes could be selectively obtained by varying the NaOH concentration and hydrothermal temperature. For example, CeO_2 nanorods were yielded at a much higher concentration (C_{NaOH} = 6 – 9 mol L^{-1}) when hydrothermally treated at 100°C, while CeO_2 nanocubes were formed under the same reactant concentrations but 180°C. The base concentration and hydrothermal temperature seemed to be the two key factors in the selective formation of CeO_2 nanopolyhedra, nanorods, and nanocubes according to Table II-I.

TABLE II-I

CRYSTAL STRUCTURES, SHAPES, AND SIZES OF SEVERAL CeO_2 SAMPLES (MAI, 2005)

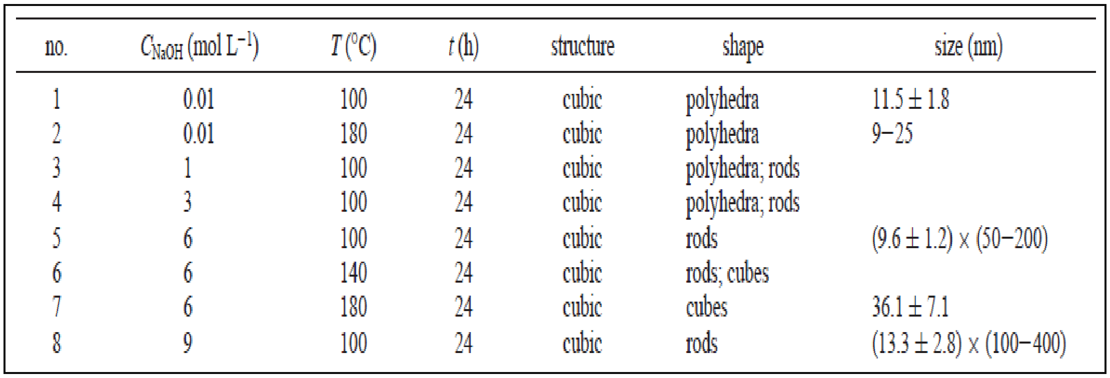

no.	C_{NaOH} (mol L^{-1})	T (°C)	t (h)	structure	shape	size (nm)
1	0.01	100	24	cubic	polyhedra	11.5 ± 1.8
2	0.01	180	24	cubic	polyhedra	9–25
3	1	100	24	cubic	polyhedra; rods	
4	3	100	24	cubic	polyhedra; rods	
5	6	100	24	cubic	rods	(9.6 ± 1.2) x (50–200)
6	6	140	24	cubic	rods; cubes	
7	6	180	24	cubic	cubes	36.1 ± 7.1
8	9	100	24	cubic	rods	(13.3 ± 2.8) x (100–400)

On the other hand, CeO_2 nanowires (Tana, 2009) exhibited a much higher OSC than the nanorods despite their comparable specific surface area and similar geometrical configuration. The higher OSC might be due to the differing proportions of exposed (1 1 0) and/or (1 0 0) planes between the nanorods and the nanowires. Since the OSC on the (1 0 0) plane is much higher than that on the (1 1 0) plane in CeO_2, it is most likely that the nanowire exposes relatively more (1 0 0) planes on the surface than the nanorod, although both of them preferentially expose the (1 1 0) and (1 0 0) planes, as shown in Figure 2.5 (c) to (f).

CeO_2 nanocubes are formed not only due to the accelerated dissolution/recrystallization, but also due to a transfer step from $Ce(OH)_3$ to CeO_2.

Nanocubes resulted at higher base concentrations as temperature was raised from 100 to 180°C. It is enclosed by six (100) planes and that {100}/ {110}-dominated surface structures are much more reactive for CO oxidization and make the associated lattice oxygen migration from bulk to surface much easier than the {111}-dominated one, and the {100}-dominated one is more active than the {110}- dominated one (Madier, 1999).

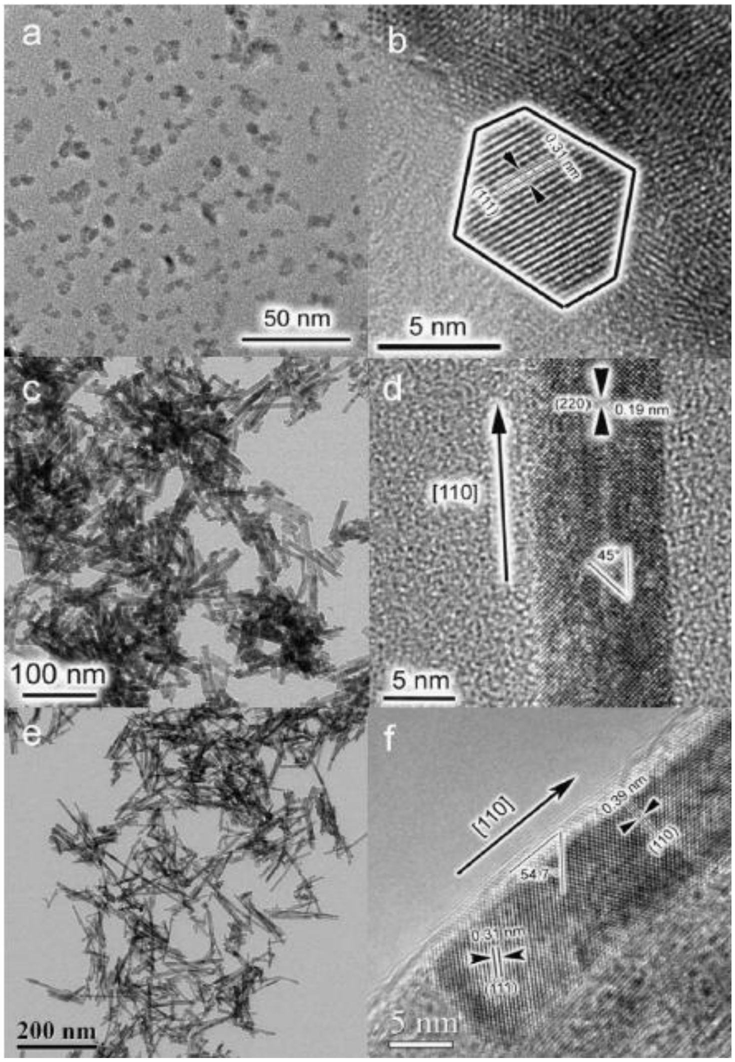

FIGURE 2.5 - TEM images of the CeO2 nanoparticles (a and b), nanorods (c and d) and nanowires (e and f) (Tana, 2009).

Other approaches or recent studies in CeO_2 have focused on the size/shape-controlled nanostructures. For example, Chen et al. (2004) fabricated polycrystalline CeO_2 nanowires via a solution-phase route using sodium bis(2-ethylhexyl) sulfosuccinate as a structure-directing agent, and observed size-dependent effect on Raman spectra. Wu et al. (2004) obtained fluorite-type ceria nanowires with diameters of 70 nm by a sol-gel process within the nanochannels of porous anodic alumina (a "hard" template). Li et al. (2005) synthesized single-crystalline CeO_2 nanorods by hydrothermal method, which showed an enhanced CO conversion activity. Yang et al. (2006) produced CeO_2 nanocubes through a solvothermal approach using oleic acid as stabilizing agent while monodisperse CeO_2 nanocubes have been fabricated via an acrylamide-assisted hydrothermal route by using $(NH_4)_2Ce(NO_3)_6$ and $CeCl_3{\cdot}7H_2O$ instead of $Ce(NO_3)_3{\cdot}6H_2O$ as the cerium source which resulted in uniform spherical particles shown in Figure 2.6 with an average diameter of 200 nm.

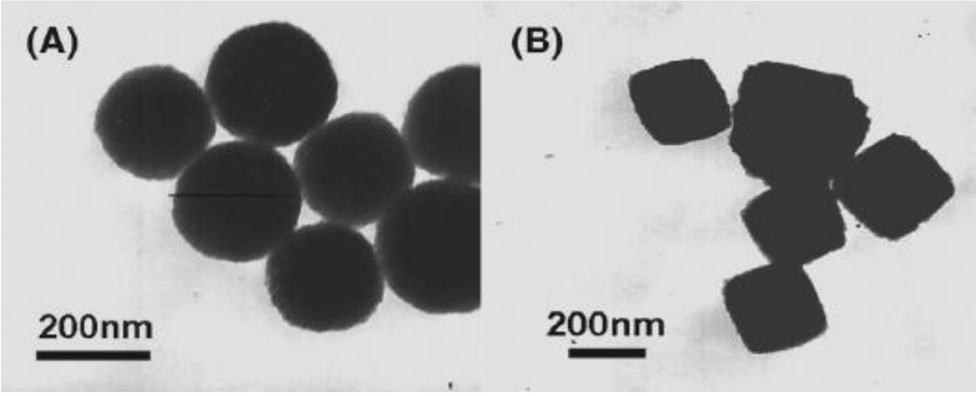

FIGURE 2.6 - TEM images of the products obtained by the utilization of varied cerium source: (A) $(NH_4)_2Ce(NO_3)_6$; (B) $CeCl_3{\cdot}7H_2O$ (Yang, 2009).

III. EXPERIMENTATION

A. Plan of Experimentation

Three different synthesis methods were designed to investigate the properties of cerium oxide nanostructures synthesized with the three precursors H_2O_2, NH_4OH, and NaOH. The synthesis was performed by hydrothermal reaction at temperatures 100, 180, and 220^{o}C. The experimental flow chart in Figure 3.1 illustrates the schematic procedure of the synthesis of CeO_2 by hydrothermal method using H_2O_2. The details of the different parameters used to synthesize the different ceria nanostructures are presented in the Procedure Section of this chapter.

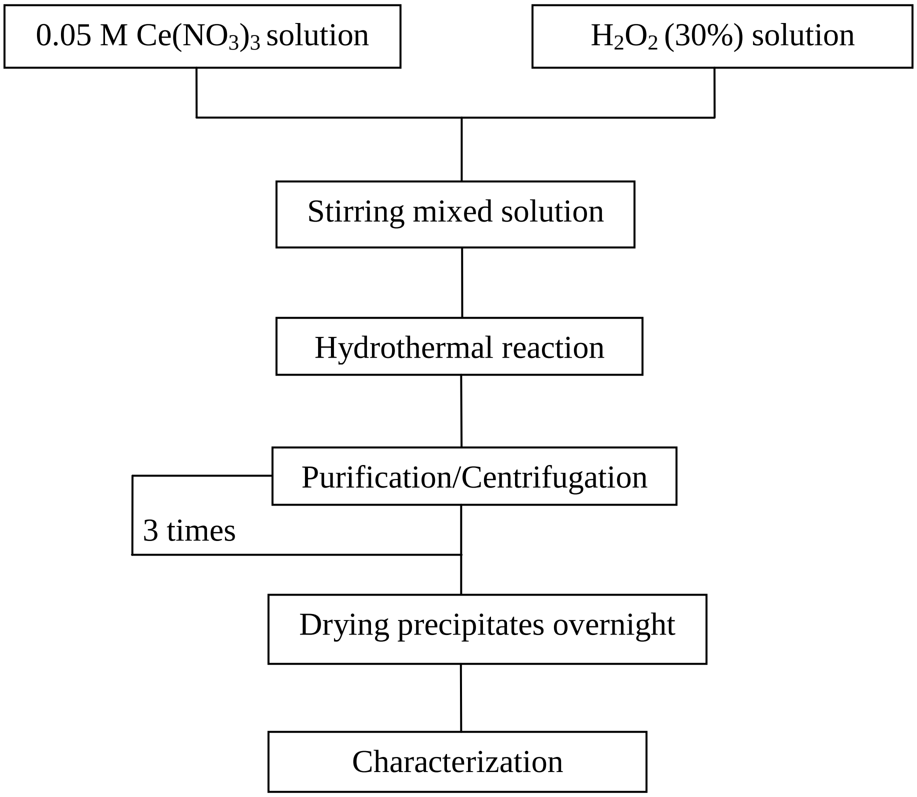

FIGURE 3.1 - Experimental flow chart of synthesis of CeO_2 with H_2O_2.

In order to identify the morphology of ceria, characterization was performed through BET specific surface area, transmission electron microscopy (TEM), X-ray photoelectron spectroscopy (XPS), and X-ray diffraction (XRD). TEM, XPS and XRD equipments are illustrated in Figures 3.3 – 3.5. It was found that the synthesis of ceria produces nanoplates, nanorods, and nanocubes depending on the type of precursor used and other parameters such as reaction time and concentration.

B. Materials

Source:

Cerium (III) nitrate hexahydrate, 99% metal basis (0.05 M $Ce(NO_3)_3$)
Sigma-Aldrich, Inc
St Louis, MO 63103 USA
Product of China
Cat. No.: 238538-100G

Precursors:

Perdrogen® 30% by weight H_2O_2 puriss. p.a.
Reag. ISO, Reag. Ph. Eur. Stabilized, (Hydrogen Peroxide)
Sigma-Aldrich, Inc
St Louis, MO 63178 USA
Made in Germany
Cat. No.: 31642

Sodium Hydroxide, pellets, 99.99% metals basis,
semiconductor grade (Na_2CO_3 < 1%)
Sigma-Aldrich, Inc
St Louis, MO 63103 USA
Product of USA
Cat. No.: 306576-100G

Ammonium Hydroxide, A.C.S. reagent (28%)
Sigma-Aldrich, Inc
St Louis, MO 63103 USA
Product of USA
Cat. No.: 306576-100G

Deionized water

C. Procedure

The hydrothermal synthesis of cerium oxide was conducted in a 50 ml Teflon autoclave shown in Figure 3.3 and then heated up to 100, 180, and 220^{o}C in a furnace, Figure 3.3, for 24 hours. First, a 50 ml solution of 0.05 M Ce $(NO_3)_3$ was prepared. The weight of 0.05 M Ce $(NO_3)_3$ for the 50 ml solution was 1.085 g. This solution was used to react with H_2O_2 or NH_4OH to form ceria nanoplates.

Table III-I through table III-IV present the three methods of synthesis that were performed; they differ because of the precursors used for the formation. In this study, ceria nanoplates, nanorods, and nanocubes are produced by the following the synthesis recipes.

TABLE III-I

SYNTHESIS OF CERIA NANOPLATE WITH HYDROGEN PEROXIDE PRECURSOR (TANG, 2005)

Vol. 30% H_2O_2	8 ml
Solution 0.05 M $Ce(NO_3)_3$	8 ml
Stirring time	10 min
Temperature	220^{o}C
Time	24 h

TABLE III-II

SYNTHESIS OF CERIA NANOPLATE WITH AMMONIUM HYDROXIDE PRECURSOR

Vol. NH_4OH (28%)	10 ml
Solution 0.05 M $Ce(NO_3)_3$	10 ml
Stirring time	10 min
Temperature	100^{o}C
Time	24 h

TABLE III-III

SYNTHESIS OF CERIA NANOROD (C_{NaOH}=9M) WITH SODIUM HYDROXIDE PRECURSOR (MAI, 2005)

Weight of 0.05 M $Ce(NO_3)_3$	0.86 g
DI water	5 ml
Weight of NaOH pellets	≈12.68 g
DI water	35 ml
Total mixed solution	40 ml
Stirring time	30 min
Temperature	100^oC
Time	24 h

TABLE III-IV

SYNTHESIS OF CERIA NANOCUBE (C_{NaOH}=6M) WITH SODIUM HYDROXIDE PRECURSOR (MAI, 2005)

Weight of 0.05 M $Ce(NO_3)_3$	0.86 g
DI water	5 ml
Weight of NaOH pellets	≈8.46 g
DI water	35 ml
Total mixed solution	40 ml
Stirring time	30 min
Temperature	180^oC
Time	24 h

After the hydrothermal synthesis, the precipitates were separated by centrifugation and washed with deionized water several times. In order to characterize, precipitates were dried overnight at 75^oC. The precipitates turned into yellow and white powders for NaOH precursor at 6M and 9M, respectively, white for H_2O_2 and dark yellow for NH_4OH. For XRD, CeO_2 powders were calcined at 100^oC, 400^oC, and 600^oC for 12 hours.

D. Characterization of the Prepared CeO_2

The crystallinity of final CeO_2 nanostructures was recorded by XRD (D8 Dicover) shown in Figure 3.6 using CuKα radiation ($\lambda = 1.5406$ Å) in the 2θ range of 20-90^o at 0.02^o 2θ/s. To estimate crystallite size and lattice parameter, the reflection from (111) plane was used for the analysis. Particle morphology, state of agglomeration and crystalline state were determined by transmission electron microscopy (TEM) shown in Figure 3.4. The Brunaure Emmett Teller (BET) specific surface area was measured by nitrogen-adsorption-desorption isotherms at 77.3 K with TriStar 3000. X-ray photoelectron spectra (XPS) shown in Figure 3.5 were measured by employing Mg-Kα radiation (BE = 1253.6 eV). The binding energy (BE) was calibrated by setting the BE of Ce 3d, O 1S, and C 1S to 935-875, 545-525 and 295-275 eV, respectively.

E. Equipment

Ney® Vulcan 3-550 Furnace
Dentsupply Ceramco International
York, PA 17404
Mfg No.: AKW0917113
Serial No.: 9493308

FIGURE 3.2 – Vulcan Furnace

Teflon autoclave (50 ml)

FIGURE 3.3 – Hydrothermal Autoclave

Tecnai F20
FEI Company
Made in USA

FIGURE 3.4 - Transmission Electron Microscopy

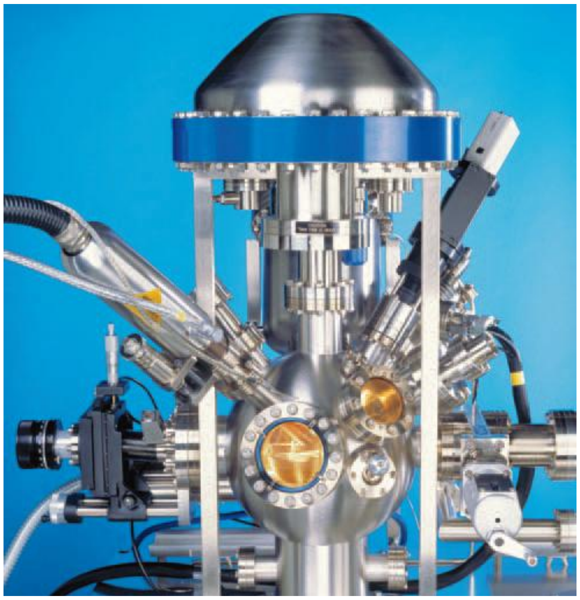

Thermo VG Scientific
Product Type: Multilab
Serial No.: A1126
The Birches Industrial Estate
West Sussex, United Kingdom RH91UB

FIGURE 3.5 - X-ray Photoelectron Spectroscopy

Bruker AXS – Diffraktometer D8
Erz Nr.: 7KP2025 – 2LR15-0Z
Serial No.: 203407
Karlsruhe, Germany D76181

FIGURE 3.6 - X-ray diffraction

IV. RESULTS AND DISCUSSION

A. Shape Selective Synthesis and Its Mechanism

Previously, it was stated that ceria nanoplates, nanocubes and nanorods were fabricated by using three different precursors (H_2O_2, NH_4OH, and NaOH) and using $Ce(NO_3)_3$ as the cerium source. In this work, we found that CeO_2 nanoplates using H_2O_2 and NH_4OH are obtained in the investigated temperature range from 100^oC to 250^oC. In the case of nanoplates using H_2O_2, increasing the hydrothermal temperature or decreasing the time does not affect the crystal structure. Furthermore, nanorods and nanocubes could be selectively fabricated by changing the base concentrations of NaOH and hydrothermal temperature. CeO_2 nanocubes were synthesized at a hydrothermal temperature of 100^oC with a base concentration (C_{NaOH} = 6 M) whereas, the elevated concentration (C_{NaOH} = 9 M) led to the formation of CeO_2 nanorods. According to the results discussed later, the base concentration and hydrothermal temperature seem to be the two key factors in the selective formation of CeO_2 nanocubes and nanorods.

In the following, a sequence of reaction condition-dependent experiments were conducted to understand the characteristics of the nucleation and crystal growth processes involved in the synthesis and further to uncover the underlying shape-selective mechanism. Details of ceria characterization and analysis of the different morphologies help to understand this phenomenon.

B. TEM analysis

A TEM image of CeO_2 nanoplates using H_2O_2 as oxidizing agent shown in Figure 4.1 has an average particle size of 25 x 20 x 20 nm. The SAED (selected area electron diffraction) pattern shows that the nanoplates were composed of cubic fluorite-type CeO_2 described later. Three kinds of lattice fringe directions attributed to (111), (200), and (220) were observed for these nanoplates, which have respective interplanar spacing of 0.31, 0.27, and 0.19 nm calculated using Bragg's Law discussed in the section E. XRD analysis.

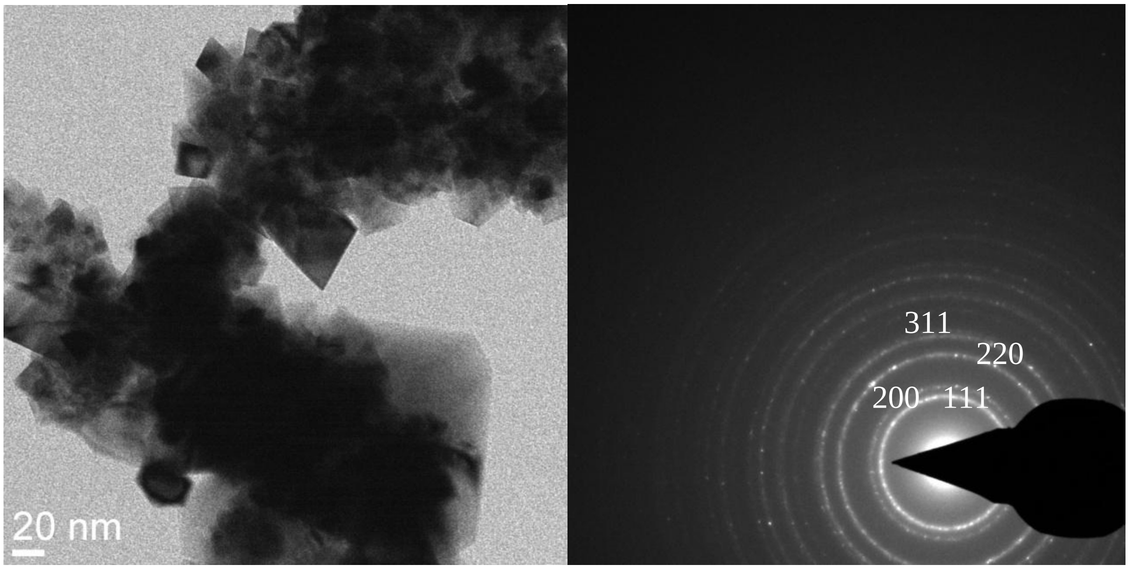

FIGURE 4.1 - TEM and SAED images of CeO_2 nanoplates at 220°C by H_2O_2.

CeO_2 nanoplates were formed using H_2O_2 at different temperatures but maintaining the same concentration to see if the synthesis temperature has an effect on ceria crystal structure. However, it did not show any difference by synthesizing at temperatures of 180°C and 200°C, for 24 hours. Also, it did not show any effect at 250°C by changing the hydrothermal time to 3 hours as shown in Figure 4.2. They all present uniform nanoplate structure which indicate that temperature did not have an effect in the nanoceria structure using H_2O_2.

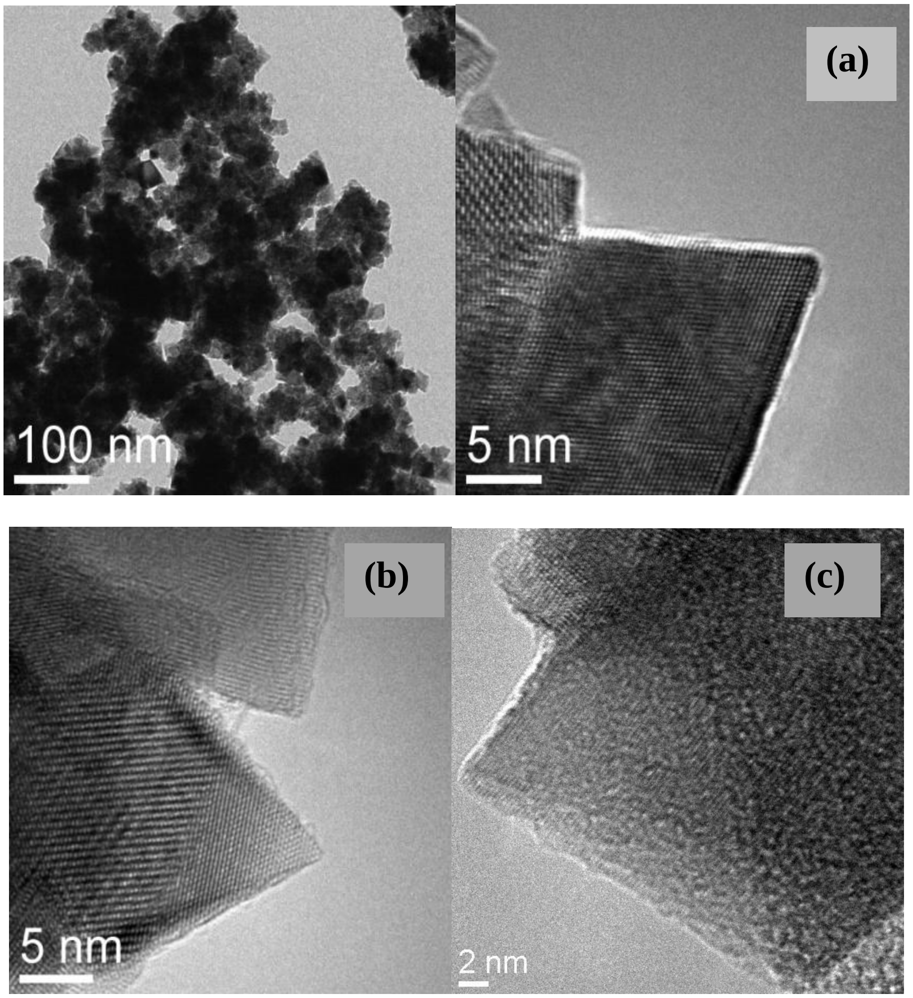

FIGURE 4.2 - TEM, HRTEM and SAED images of CeO_2 nanoplates by H_2O_2 synthesized at different temperatures (a) 180°C for 24 hr, (b) 200°C for 24 hr, and (c) 250°C for 3h.

Ceria nanoplates were formed by using NH_4OH as mentioned previously. Figure 4.3 shows ceria nanoplates synthesized at 100°C and agglomeration can be seen. Agglomeration usually increases with decrease in particle size due to higher surface energy (Tok, 2007). Nanoplates synthesized by NH_4OH also exhibit the lattice planes

(111), (200), and (220), same interplanar spacings and has a BET surface area of 62.01 m^2/g which will be explained further.

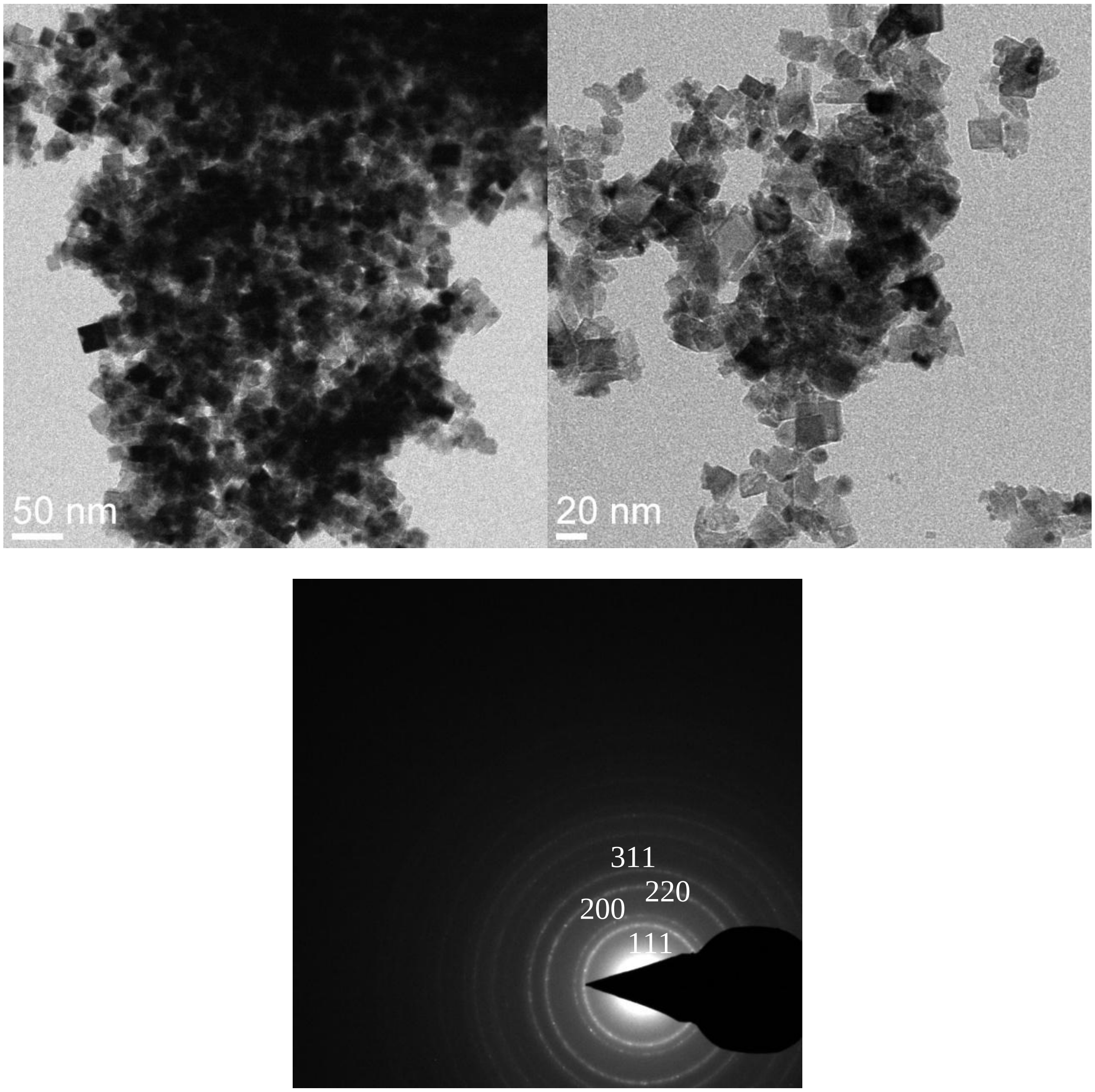

FIGURE 4.3 - TEM and SAED image of CeO_2 nanoplates by NH_4OH at 100^oC.

Figure 4.4 depicts the TEM and HRTEM images of CeO_2 nanorods using NaOH as the precursor with a concentration of 9 M. Nanorods show a 1D growth structure with a preferred growth direction along [110], and are enclosed by (220) and

(200) planes in other studies (Mai, 2005). In this study, nanorods are enclosed by the lattice planes (111), (200) and (220) according to FFT (fast Fourier transform) analysis, inset in Figure 4.4, with the direction along the [110]. Nanorods exposed the most the (111) plane with an interplanar spacing of 0.31 nm. The nanorods have an average diameter 12-20 nm and a length from 100 to 200 nm.

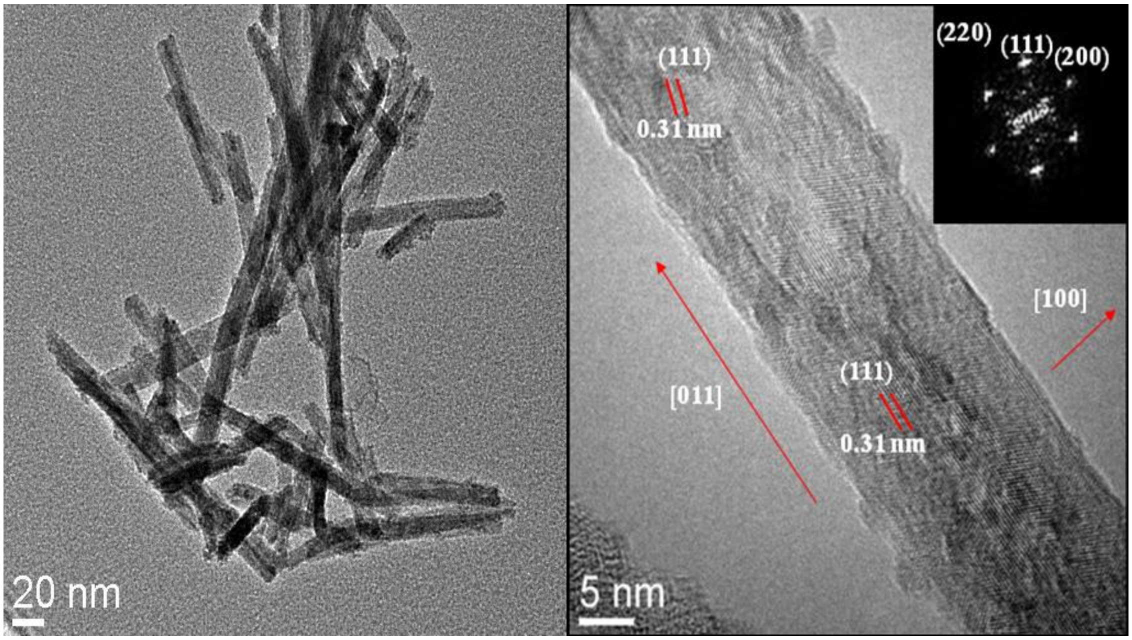

FIGURE 4.4- TEM and HRTEM images of CeO_2 nanorods with a C_{NaOH}= 9 M at 100°C.

In addition, ceria was synthesized by keeping the same concentration of NaOH (9 M) and changing the hydrothermal temperature to 180°C instead of 100°C. The crystal structure changes from nanorods to nanocubes. TEM and HRTEM images of ceria nanocubes are shown in Figure 4.5. This result indicates that temperature does have an effect on the crystal structure. The average size of nanocubes is about 40 x 40 x 30 nm. We can see that ceria nanocubes can also be fabricated either using a C_{NaOH} = 9 M at 180°C or C_{NaOH}= 6 M at 100°C.

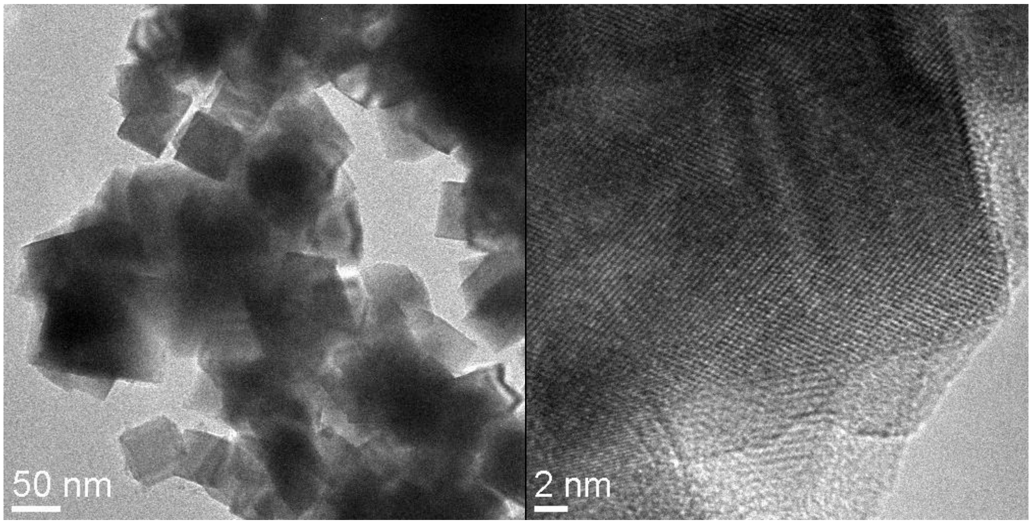

FIGURE 4.5 - TEM and HRTEM images of CeO_2 nanocubes with a C_{NaOH}= 9 M at 180^{o}C.

As mentioned earlier, ceria nanocubes are developed by using NaOH with a concentration of 6 M at hydrothermal temperature at 100^{o}C. Figure 4.6 illustrates the TEM and HRTEM images of CeO_2 nanocubes with an average size of 30 x 30 x 20 nm. Through FFT analysis, nanocubes are enclosed by the (111), (200), and (220) planes. The HRTEM displays the clear (111) lattice fringe in the directions [100] and [011] with an interplanar spacing of 0.31 nm. Other studies imply that CeO_2 nanocubes are only enclosed by the (200) planes (Mai, 2005). The TEM and HRTEM images of CeO_2 nanoplates, nanorods, and nanocubes in Figures 4.1 to 4.6 show that they are of single crystalline nature.

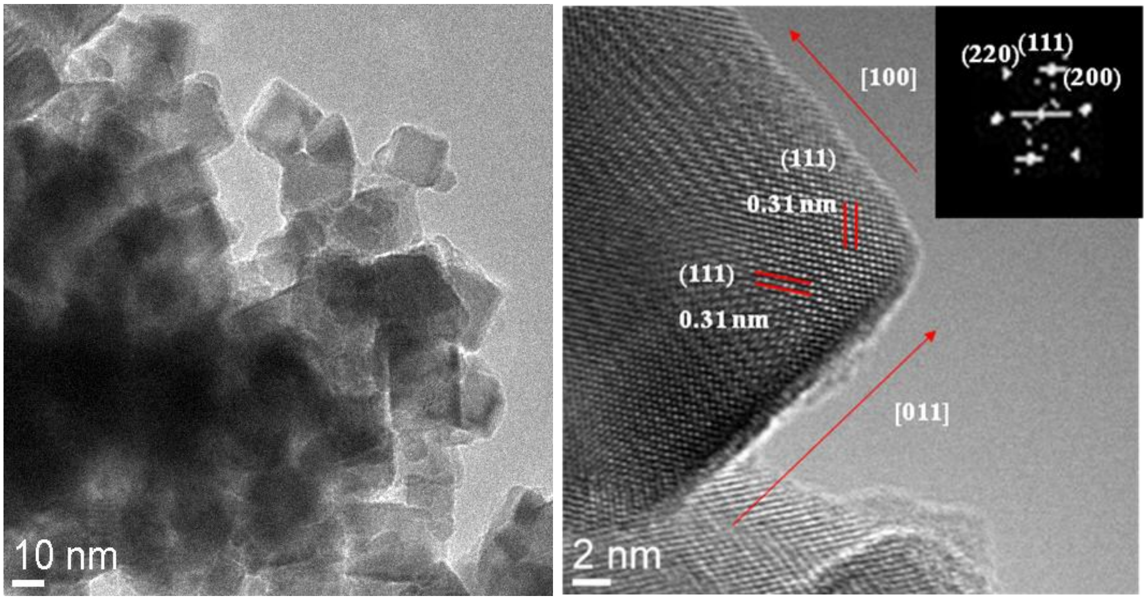

FIGURE 4.6 - TEM and HTERM images of CeO_2 nanocubes with a C_{NaOH}= 6 M at 180°C.

C. BET specific surface area analysis

Brunaure Emmett Teller (BET) analysis was performed to measure the surface area of different CeO_2 nanostructures. Table IV-I reports the BET specific surface area of ceria nanoplates, nanocubes and nanorods. Nanoplates show a higher surface area while nanorods and nanocubes have lower surface area. Ceria nanostructures need to have a high surface area because of their importance in industrial applications such as catalyst. In the present work, nanorods and nanocubes show a low surface area, and, as a result, CeO_2 nanoplates could be better catalyst from surface area aspect. CeO_2 nanoplates have high surface area than nanocubes and nanorods. Nanorods and nanocubes have compatible surface area even though they are of different morphology.

TABLE IV-I

BET SPECIFIC SURFACE AREA OF DIFFERENT CeO_2 SHAPES

Precursor	H_2O_2	NH_4OH	NaOH-6M	NaOH-9M
Shape	Nanoplate	Nanoplate	Nanocube	Nanorod
BET surface area (m^2/g)	95.11	62.07	16.55	16.74

The N_2 adsorption-desorption isotherm plots are illustrated in Figure 4.7. The hysteresis loop at P/P_o 0.8-1.0 of Fig. 4.7c indicates that nanocubes elucidate the typical IUPAC type IV pattern (Pavasupree, 2006), revealing the presence of mesoporous material. The isotherm for nanorods in Fig. 4.7d exhibits also type IV pattern with variation of nitrogen adsorbed volume at P/P_o 0.4-0.9 indicating also the existence of mesopores. However, BET surface area does not correlate with the existence of mesoporous material for nanorods and nanocubes because they show small surface area.

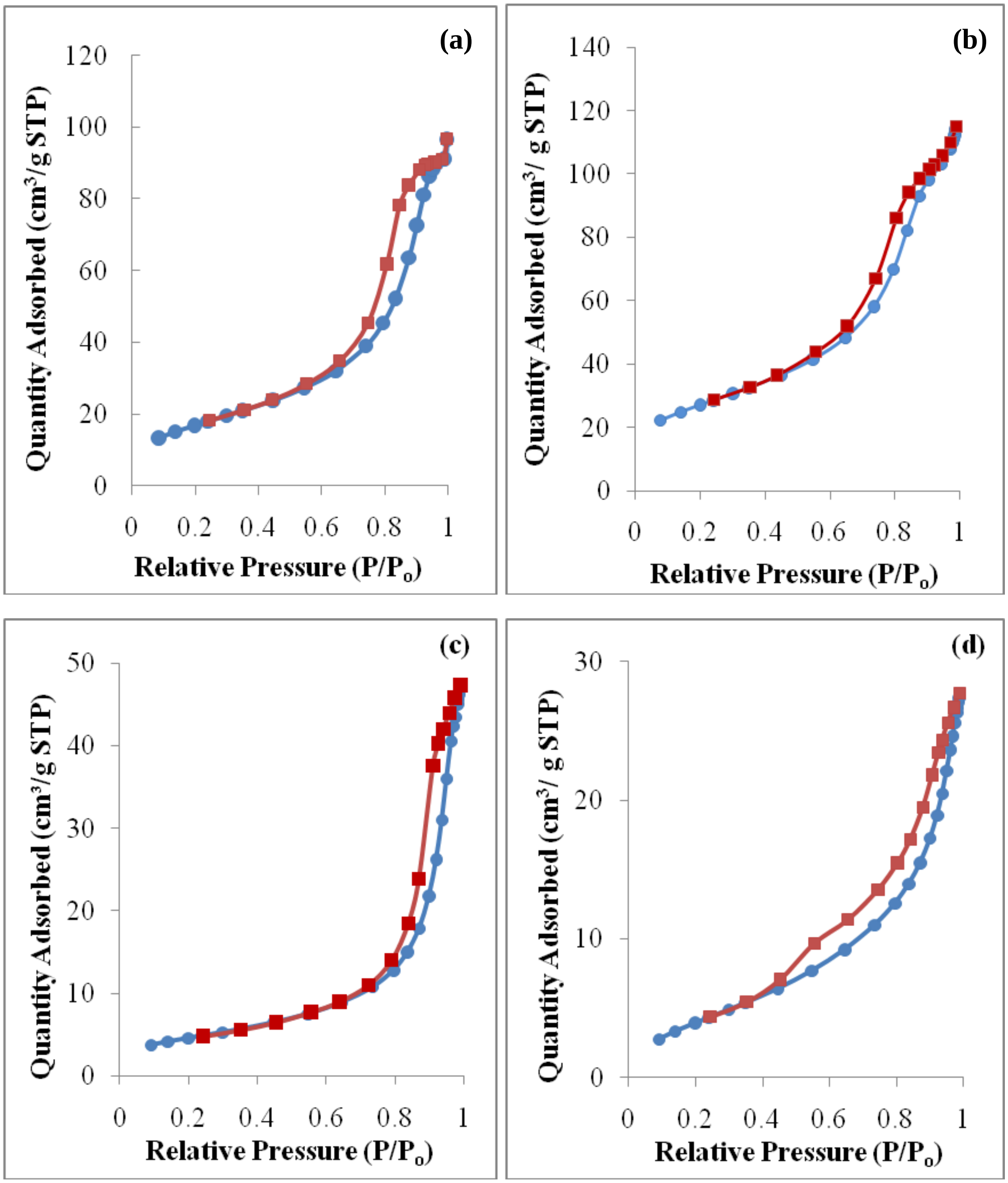

FIGURE 4.7 - Nitrogen adsorption-desorption isotherm pattern as synthesized of CeO_2 nanoplates using H_2O_2 (a), nanoplates using NH_4OH (b), nanocubes (c), and nanorods (d), (● adsorption, ■ desorption).

Nanoplates also present a typical type IV pattern with hysteresis loop as shown in Fig. 4.7a-b, which is characteristic of mesoporous material according to the classification of

IUPAC. Characteristic features of the Type IV isotherm are its hysteresis loop, which is associated with capillary condensation taking place in mesopores. Type IV isotherms are given by many mesoporous industrial adsorbents (Sing, 1985). A sharp increase in adsorption volume of N_2 was observed and located in the P/P_o range of 0.70-0.85. This sharp increase can be attributed to the capillary condensation, indicating a good homogeneity of the sample and fairly small pore size since the P/P_o position of the inflection point is related to the pore dimension (Pavasupree, 2006). The pore size distribution based on Barret-Joyner-Halenda (BJH) model of CeO_2 at different shapes is shown in Figure 4.8.

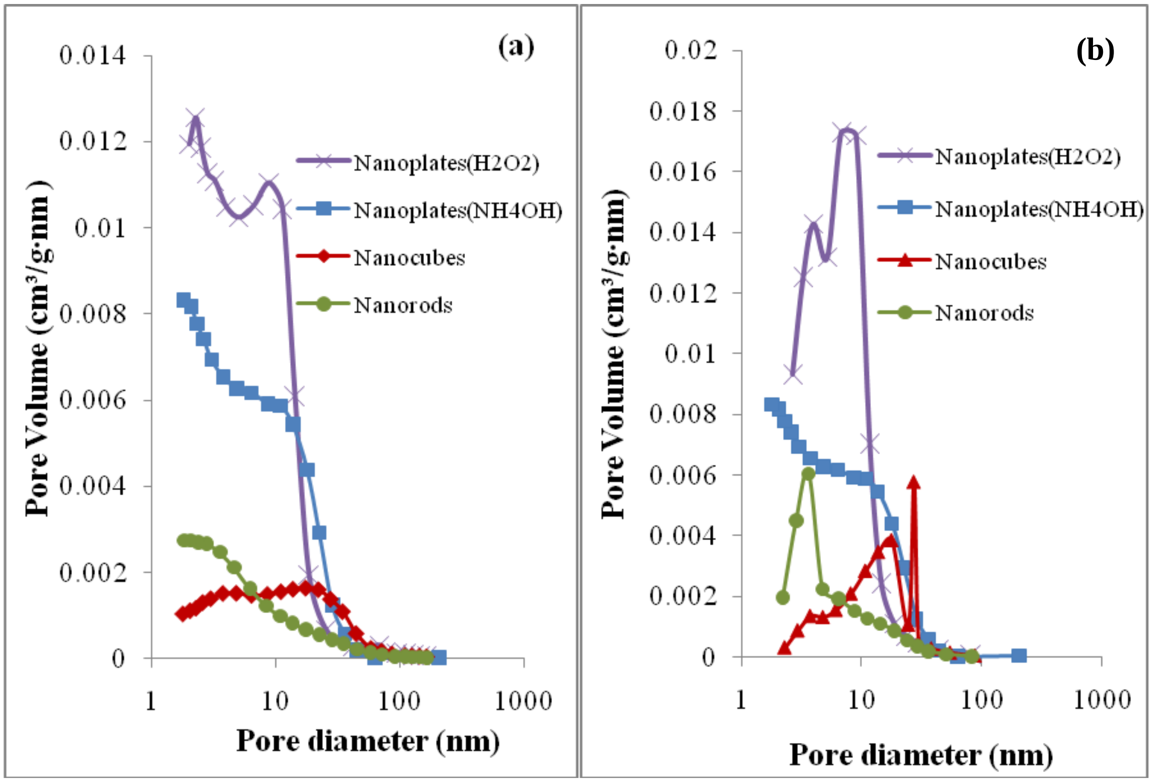

FIGURE 4.8 - Plot of the pore volume vs. pore diameter for CeO_2 nanoplates by H_2O_2, nanoplates by NH_4OH, nanocubes, and nanorods in BJH adsorption (a) and desorption (b).

We can see from Figure 4.8 of adsorption and desorption pore diameter distribution that the application of BJH model to desorption branch will give a completely different result compared to that of the adsorption branch. Similar phenomena have been observed by others (Groen, 2003). In desorption branch, nanocubes and nanorods isotherms have narrower pores centered on 13 nm and 7 nm, respectively. However, in the adsorption branch, nanorods and nanocubes show a broad distribution centered approximately 17 nm and 9 nm, respectively. Nanoplates by NH_4OH derived from the adsorption branch indicates that the created mesopores show a semi-narrow distribution by having an average pore diameter of about 8-9 nm while nanoplates by H_2O_2 had about 7-8 nm. The pore sizes of the CeO_2 nanomaterials are within the mesopores range 2-50 nm (Sing, 1985), which prove that they are of mesoporous material. Table IV-II summarizes the pore diameter and pore volume for the ceria structures studied by BJH adsorption.

TABLE IV-II

AVERAGE PORE SIZE AND PORE VOLUME OF THE PREPARED CERIA NANOMATERIALS

Precursor	Shape	Pore Volume by BJH Adsorption (cm^3/g)	Pore size by BJH Adsorption (nm)
H_2O_2	Nanoplate	0.179	7.33
NH_4OH	Nanoplate	0.149	8.54
NaOH-6M	Nanocube	0.073	14.75
NaOH-9M	Nanorod	0.042	8.52

D. XPS analysis

X-ray photoelectron spectroscopy (XPS) was conducted in the studied nanoceria structures. Figure 4.9 exhibits the XPS patterns of CeO_2 nanoplates, nanocubes, and nanorods. Peaks of Ce 3d, O 1s, C 1s, and Ce 4d can be recognized. Also, there were no peaks observed attributable to Na 2p and ammonium which means that the NaOH and NH_4OH impurities were not present.

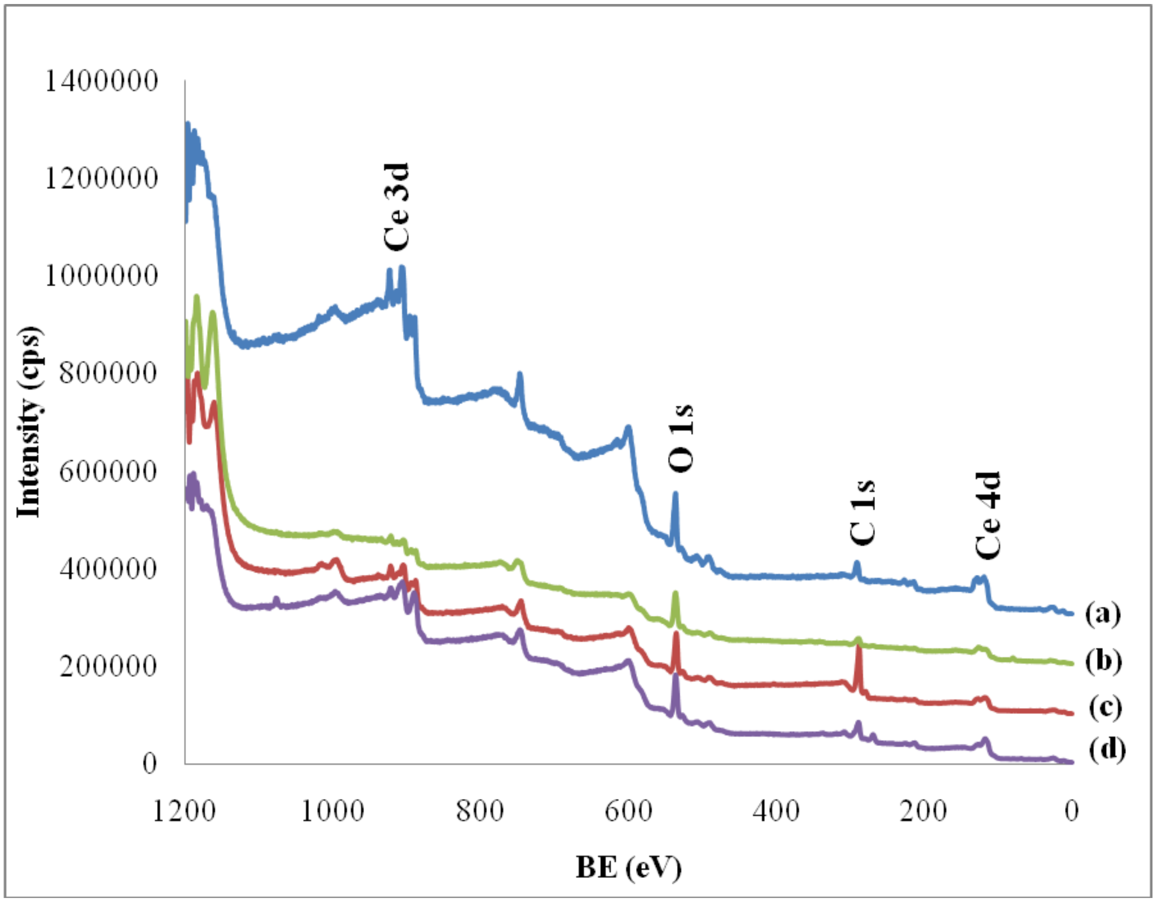

FIGURE 4.9 - XPS survey spectra of CeO_2 nanoplates by H_2O_2 (a), nanocubes (b), nanoplates by NH_4OH (c), and nanorods (d).

Moreover, Figure 4.10 indicates that six Ce 3d binding energy (BE) peaks were steady with previous studies on Ce^{4+} indicating that the main cerium valence of cerium oxide in the nanoplates, nanocubes, and nanorods was Ce^{4+}. Ceria nanoplates using H_2O_2 show a higher intensity than the rest while nanoplates using NH_4OH and nanocubes have similar intensities.

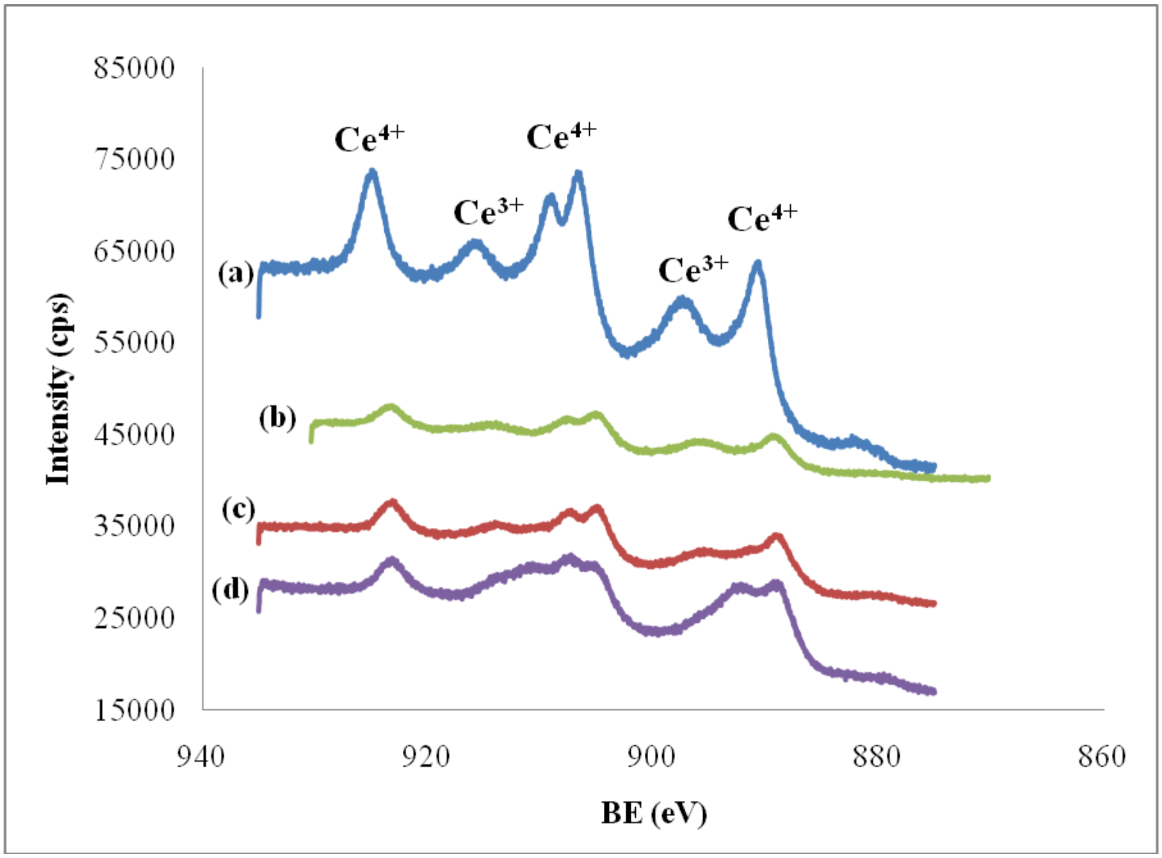

FIGURE 4.10 - XPS spectrum of the six peaks of Ce 3d for nanoplates by H_2O_2 (a), nanocubes (b), nanoplates by NH_4OH (c), and nanorods (d).

The mixed valence state (Ce^{3+} and Ce^{4+}) is illustrated in Figure 4.11 for the synthesized cerium oxide nanoplates by H_2O_2. Ceria nanoplates, nanocubes and nanorods also show the same presence of a mixed valence state. Ce^{3+} ions are introduced in the nanoceria crystal lattice because of oxygen vacancies created by surface chemical reactions (Tarnuzzer, 2005). Also, Tarnuzzer suggested that nanoceria behaves as an antioxidant due to the presence of the mixed valence states of Ce^{3+} and Ce^{4+} on the surface.

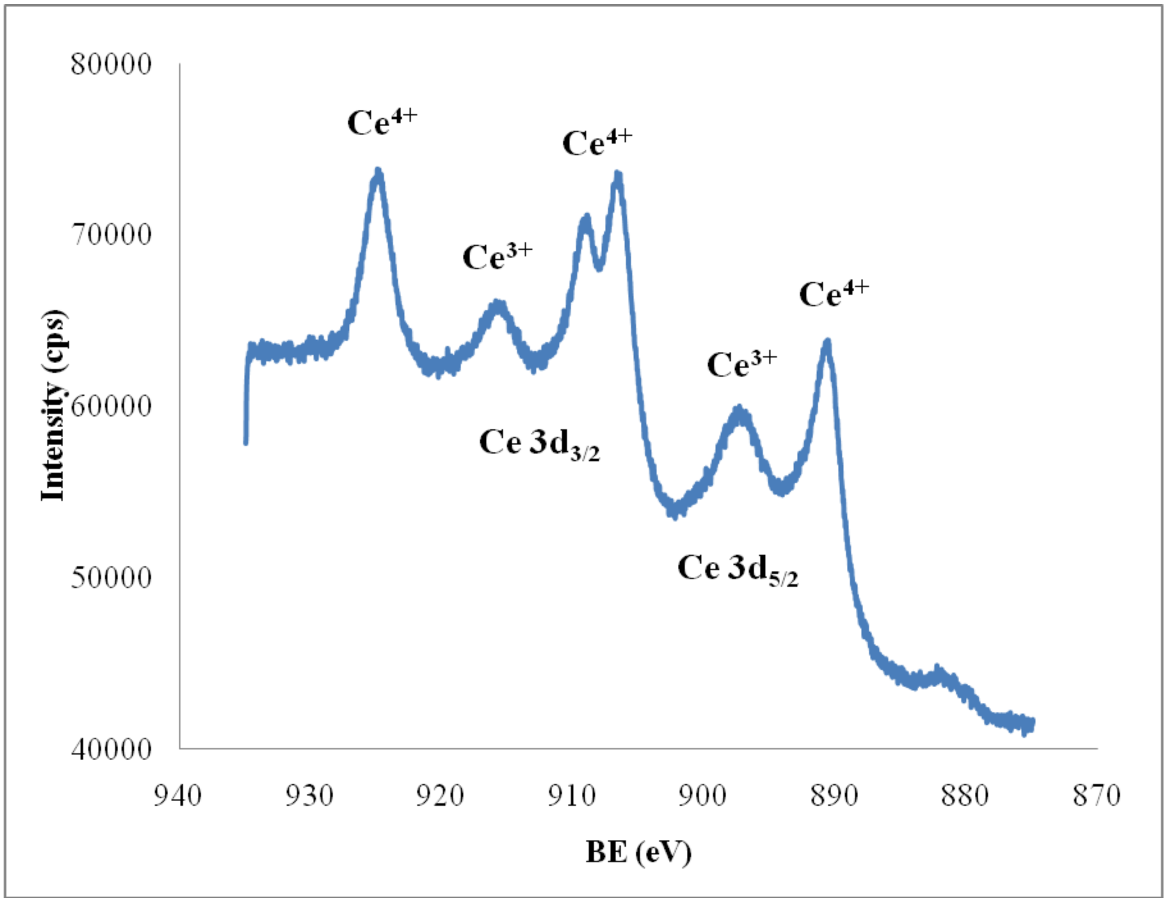

FIGURE 4.11 - XPS spectrum of the synthesized ceria nanoplates by H_2O_2 with the mixed valence state.

Deconvoluted XPS Ce (3d) spectra were performed in CeO_2 nanoplates, nanocubes, and nanorods. An example image of deconvoluted peaks of ceria nanocubes is shown in Figure 4.12. Similar peak fitting for the XPS spectra of the other CeO_2 nanomaterials are presented in Appendix 2. The peaks v_0, v', u_0, and u' are characteristic of Ce^{3+} while v'', v''', u, u'', and u''' are attributed to Ce^{4+} (Seal, 2001). In the present deconvoluted spectrums, peak *v* has a value of zero because it was not necessary to add another peak to fit it into the actual spectrum.

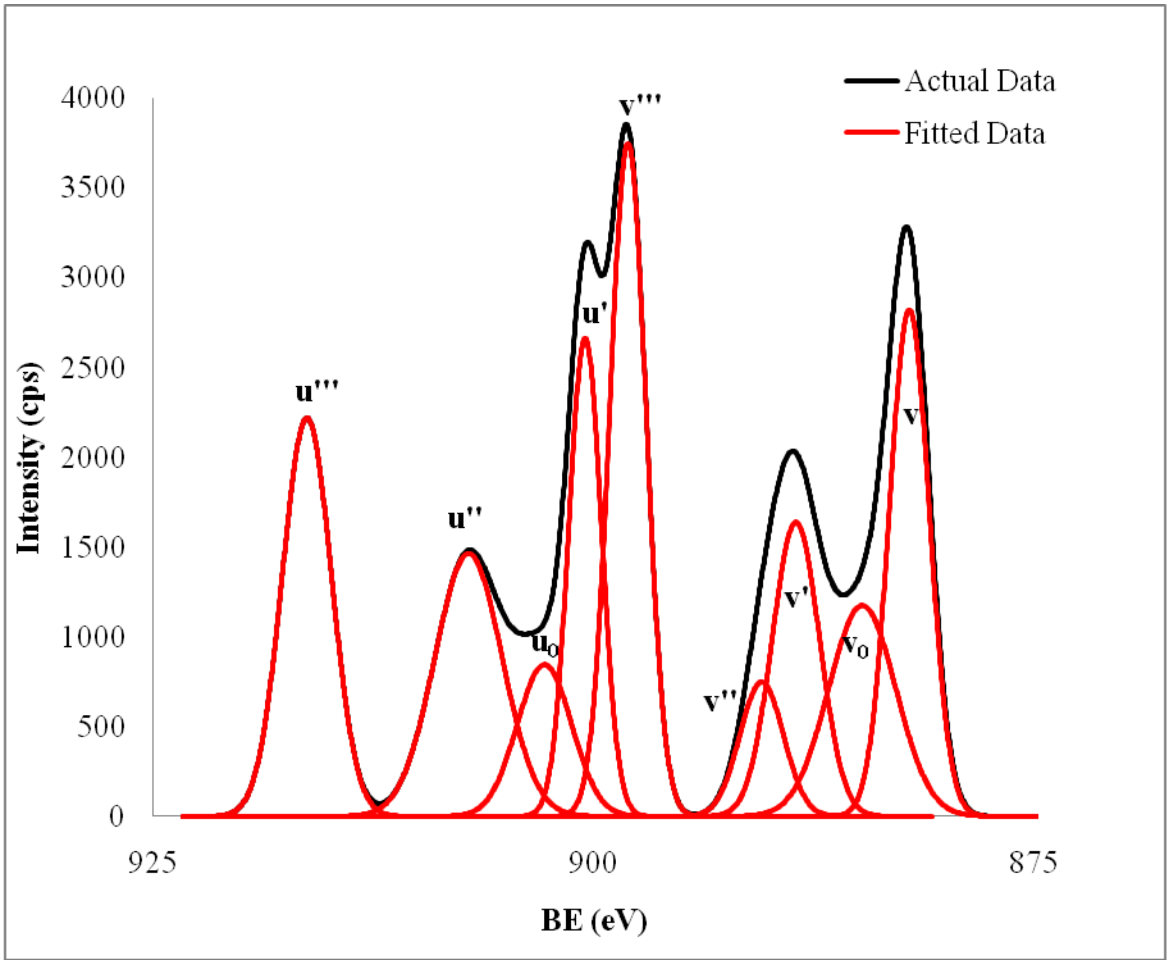

FIGURE 4.12 - Deconvoluted XPS Ce (3d) spectrum of ceria nanocubes.

The individual peak positions for all the studied nanoceria shapes are listed in Table IV-III. Notice that the values of the individual peaks are essentially identical between the different shapes of ceria which indicates that the fitted-peaks were introduced in similar positions in order to fit the actual Ce 3d spectrum.

TABLE IV-III

XPS BINDING ENERGIES OF INDIVIDUAL PEAKS OF THE CE (3D) SPECTRUM FOR DIFFERENT CeO_2 SHAPES

Shape	**Ce ($3d_{5/2}$)**				**Ce ($3d_{3/2}$)**				
	v_0	v'	v''	v'''	u_0	u	u'	u''	u'''
Nanoplate(H_2O_2)	882.32	885.17	888.39	891.00	898.40	901.07	903.61	907.07	916.72
Nanoplate(NH_4OH)	882.14	884.26	888.27	890.81	898.28	900.88	903.55	907.56	916.62
Nanocube	881.78	884.99	887.72	890.27	898.03	900.70	903.37	907.31	916.23
Nanorod	882.08	885.29	887.78	890.33	897.97	900.70	903.07	906.77	916.05

A partial quantitative analysis of the integrated peak area can provide the concentration of Ce^{3+} ions in the synthesized ceria. Equation 1 calculates the fraction of Ce^{3+} (Seal, 2001):

$$[Ce^{3+}]=\frac{A_{vo}+A_{v'}+A_{u0}+A_{u'}}{A_{vo}+A_{v'}+A_{u0}+A_{u'}+A_{v}+A_{v''}+A_{v'''}+A_{u}+A_{u''}+A_{u'''}} \qquad (1)$$

where A_i is the integrated area of peak "*i*." Table IV-IV and IV-V present the integrated areas obtained from each peak and the concentration of Ce^{3+} of ceria nanoplates, nanocubes and nanorods, respectively.

TABLE IV-IV

INTEGRATED AREAS OF INDIVIDUAL PEAKS

Shape	**Area of Peak**								
	A_{v0}	$A_{v'}$	$A_{v''}$	$A_{v'''}$	A_{u0}	A_{u}	$A_{u'}$	$A_{u''}$	$A_{u'''}$
Nanoplate (H_2O_2)	14680	11040	8354.20	15220	10500	6139.87	9474.21	8199.96	4743.22
Nanoplate (NH_4OH)	34770	30830	45370	32740	23230	27170	27840	15450	17990
Nanocube	24920	25780	10360	8266.41	25640	10910	25630	16880	13150
Nanowire	30890	20140	8610.84	12070	25920	11800	18890	20980	14730

Using Equation 1, we can calculate the concentration of Ce^{3+}. It has been reported that the concentration of Ce^{3+} increases with a decrease in particle size of nanoceria (Deshpande, 2005). In the current study, we found that nanocubes and nanorods have high concentration of Ce^{3+} and smaller particle sizes. It can be attributed to higher oxygen vacancies in the smaller particles.

TABLE IV-V

CONCENTRATION OF Ce^{3+} FOR DIFFERENT SHAPES OF CERIA CALCULATED USING EQ. (1).

Precursor	H_2O_2	NH_4OH	NaOH-6M	NaOH-9M
Shape	Nanoplate	Nanoplate	Nanocube	Nanorod
Concentration of Ce^{3+}	0.52	0.46	0.63	0.58

E. XRD analysis

The crystallite size and crystal structure of the CeO_2 nanoplates, nanocubes and nanorods are obtained by examining the XRD patterns. Figure 4.13 exhibits the XRD patterns of the CeO_2 nanomaterials after calcined at 100°C. The exposing XRD peaks correspond to the (111), (200), (220), (311), (400), (3310, (420), and (422) planes of a ceria cubic fluorite structure (space group Fm3m (225)) with an average lattice parameter *a* = 5.407 Å. The XRD peaks for nanorods (c) and nanoplates using (NH_4OH) (d) are very broad which indicates that these two morphologies have low crystallinity or contain a large portion of amorphous phase (Sujama, 2008).

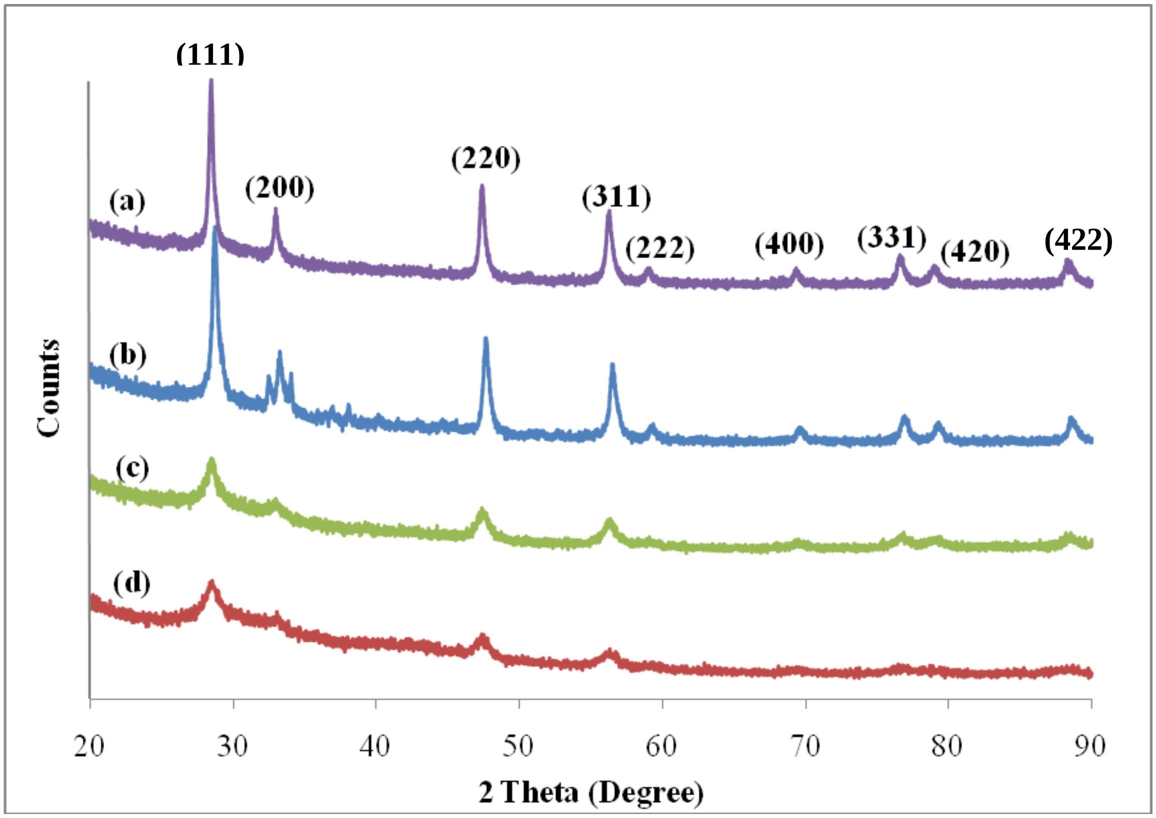

FIGURE 4.13 - XRD of CeO_2 nanoplates by H_2O_2 (a), nanocubes (b), nanoplates by NH_4OH (c), and nanorods (d).

The XRD patterns for CeO_2 nanoplates, nanocubes and nanorods calcined at 400°C and 600°C are illustrated in Figures 4.14 to 4.17. The nanoplates exhibit in Figure 4.14 using H_2O_2 show a higher intensity at 100°C than at 400°C while nanoplates using NH_4OH shown in Figure 4.15 do not present any difference between 100°C and 600°C. XRD patterns for nanocubes (C_{NaOH}=6M) shown in Figure 4.16 at 100°C shows small peaks in between the (200) plane, either another crystal structure is present or some NaOH impurities. However, at 400°C, the (200) plane shows a uniform peak which denies the fact of another crystal structure leaving the possibility of some residues of NaOH impurities in the sample. For nanorods, XRD spectrum is wider at 100°C and has lower intensity than at 600°C as shown in Figure 4.17. Narrow peaks show high crystallinity while wide peaks, low crystallinity.

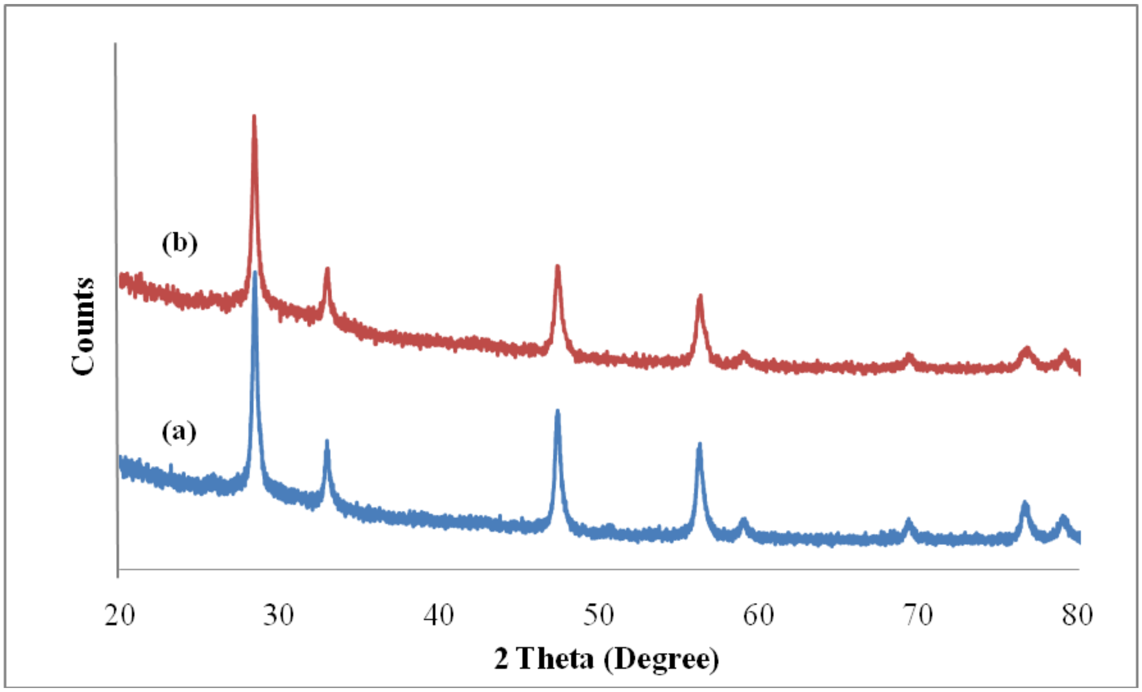

FIGURE 4.14 - XRD patterns of CeO_2 nanoplates by H_2O_2 calcined at 100°C (a) and 400°C (b).

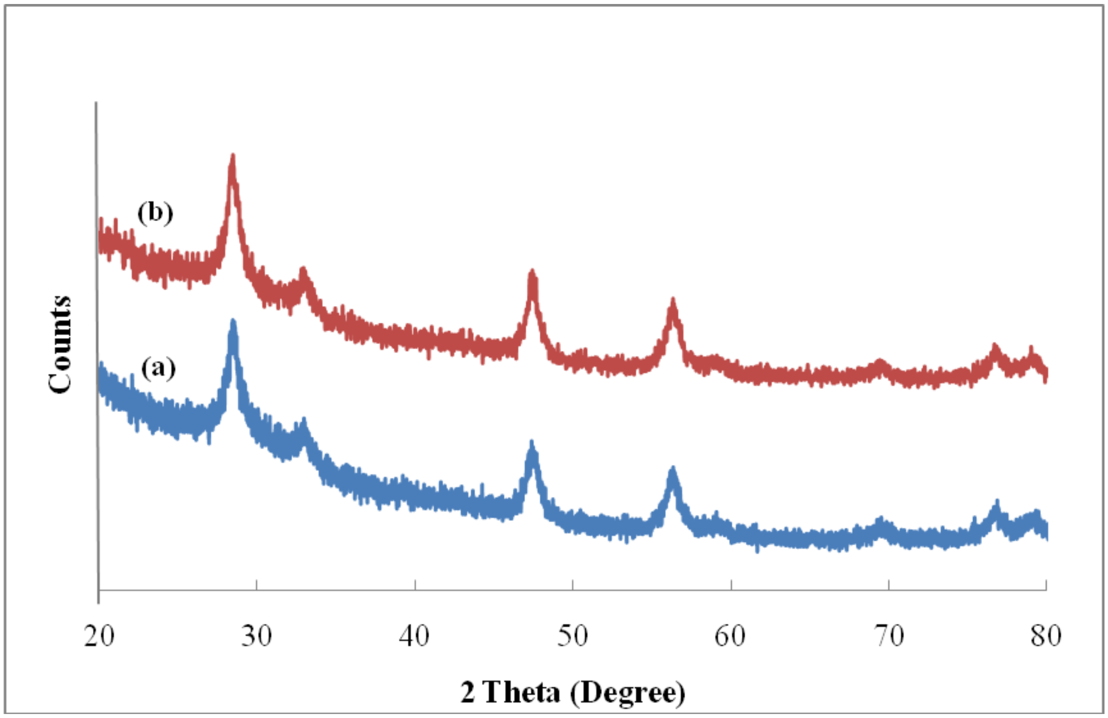

FIGURE 4.15 - XRD patterns of CeO_2 nanoplates by NH_4OH calcined at 100°C (a) and 600°C (b).

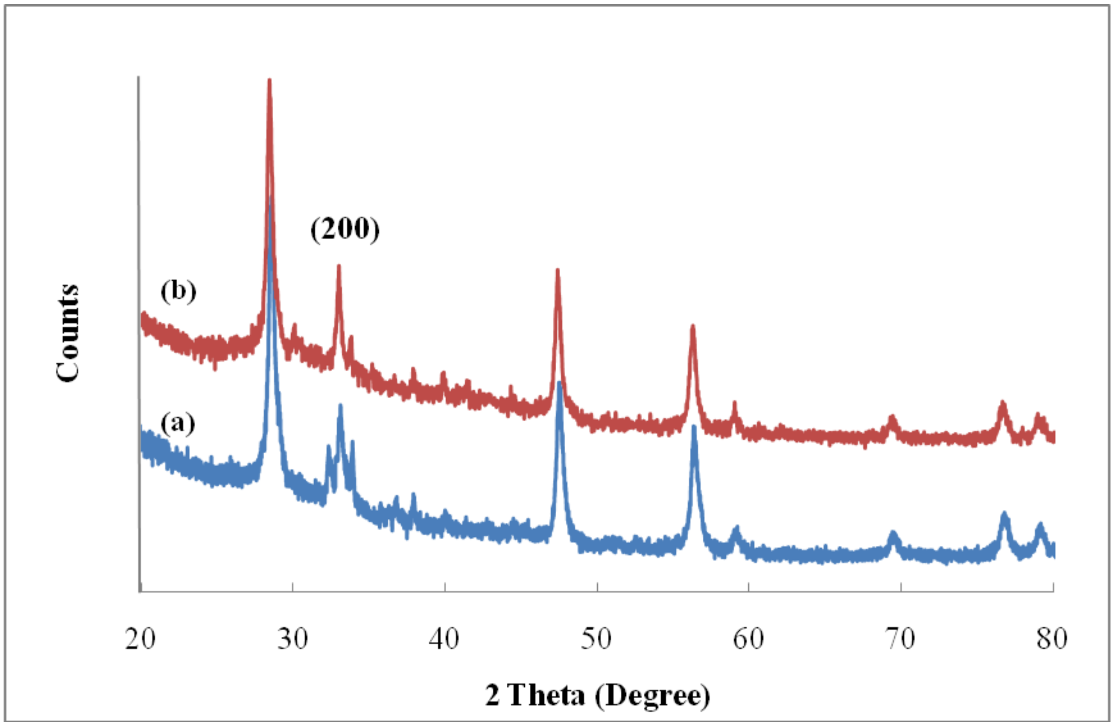

FIGURE 4.16 - XRD patterns of CeO_2 nanocubes (C_{NaOH}=6M) calcined at 100°C (a) and 400°C (b).

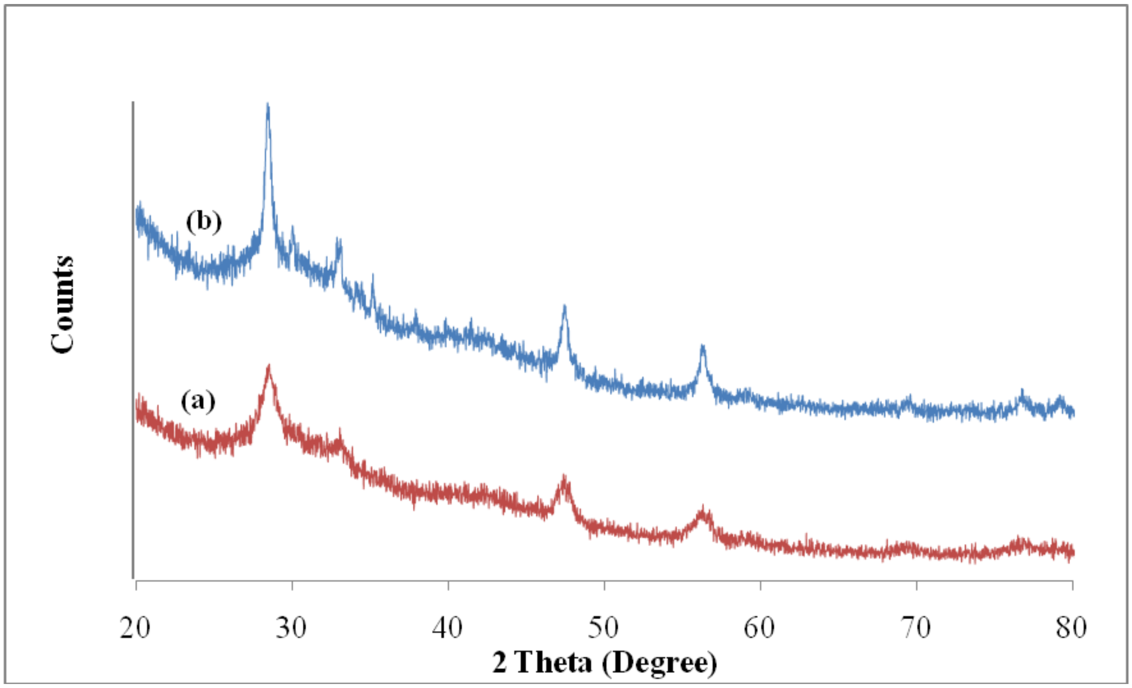

FIGURE 4.17 - XRD patterns of CeO_2 nanorods calcined at 100°C (a) and 600°C (b).

Table IV-VI shows the calculated lattice parameters, *a*, using Equation 2 versus the theoretical XRD values at different calcinations temperatures.

$$a = d_{hkl}\sqrt{h^2 + k^2 + l^2} \qquad (2)$$

The experimental lattice parameters are similar to the theoretical ones proving that the diffraction peaks correspond only to CeO_2. The different lattice parameters values are due to the different precursors used to synthesize CeO_2. It was necessary to find the right ceria pattern that belongs to ceria with its respective precursor. It is noted that some values of the lattice parameter for CeO_2 nanostructures are lower or higher than that reported for the bulk of CeO_2 which is a = 5.411 Å provided in other studies (Zhou, 2005). The lattice parameter only varied within the average range ($\Delta a/a \approx 0.25\%$). In addition, the (111) plane is the most exposing plane in the XRD spectra.

TABLE IV-VI

COMPARISON OF LATTICE PARAMETERS AT DIFFERENT CALCINATION TEMPERATURES

Precursor	Shape	100^{o}C		400^{o}C		600^{o}C	
		a, calculated	*a*, from XRD	*a*, calculated	*a*, from XRD	*a*, calculated	*a*, from XRD
H_2O_2	Nanoplate	5.4291	5.4124	5.4382	5.4124	-	-
NaOH	Nanocube	5.4035	5.4037	5.4344	5.4124	-	-
NaOH	Nanorod	5.4157	5.4037	-	-	5.4157	5.411
NH_4OH	Nanoplate	5.4291	5.4037	-	-	5.4269	5.4037

In order to calculate the crystallite size (D_{hkl}), the following equations were needed:

$$n\lambda = 2\, d_{hkl} \sin\theta \tag{3}$$

$$D_{hkl} = \frac{0.89 \times \lambda}{B_{hkl} \times \cos\theta_B} \tag{4}$$

Equation 3 expresses Bragg's Law where $n = 1$, $\lambda = 1.5406$ Å and θ is obtained from XRD spectra. The a refers to the CeO_2 FCC (face-centered-cubic) lattice parameter, and h,k,l are the crystallite size indices while d is the crystalline face space. On the other hand, Equation 4 is the Scherrer equation which is used to calculate the crystallite size (D_{hkl}) (Tennyson, 2007). The B_{hkl} corresponds to the measured half-width at maximum peak height. Table IV-VII summarizes the lattice type, lattice parameter and crystallite size values of CeO_2 nanostructures by using the equations mentioned earlier. The crystallite sizes for nanoplates, nanocubes and nanorods were estimated from X-ray line broadening of the reflections of (111) plane.

TABLE IV-VII

LATTICE TYPE AND CRYSTALLITE SIZE OF CeO_2 NANOSTRUCTURES

Shape	As synthesized			Calcined at 400°C			Calcined at 600°C		
	Lattice Type	a(Å)	D_{hkl} (nm)	Lattice Type	a(Å)	D_{hkl} (nm)	Lattice Type	a(Å)	D_{hkl} (nm)
Nanoplate (H_2O_2)	Cubic	5.4291	24.92	Cubic	5.4382	22.90	-	-	-
Nanocube	Cubic	5.4035	19.65	Cubic	5.4344	17.99	-	-	-
Nanorod	Cubic	5.4157	5.97	-	-	-	Cubic	5.4382	11.40
Nanoplate (NH_4OH)	Cubic	5.4291	12.30	-	-	-	Cubic	5.4269	12.27

The lattice type is cubic for the different morphologies of ceria. Lattice parameters values are slightly different to each other except for nanoplates by NH_4OH which are the same regardless of the calcination temperatures. Figure 4.18 illustrates the effect of calcination temperature and lattice parameter on the crystallite size. We can see that crystallite size in nanoplates using H_2O_2 shown in Fig. 4.18a increases at high calcination temperature and lattice parameter while nanoplates using NH_4OH in Fig 4.18c remain unchanged or steady, indicating that temperature and lattice parameter do not affect the size. Nanocube's crystallite size in Fig 4.18b decreases at high calcination temperature and lattice parameter while the crystallite size of nanorods in Fig 4.18d is proportional to temperature and lattice parameter.

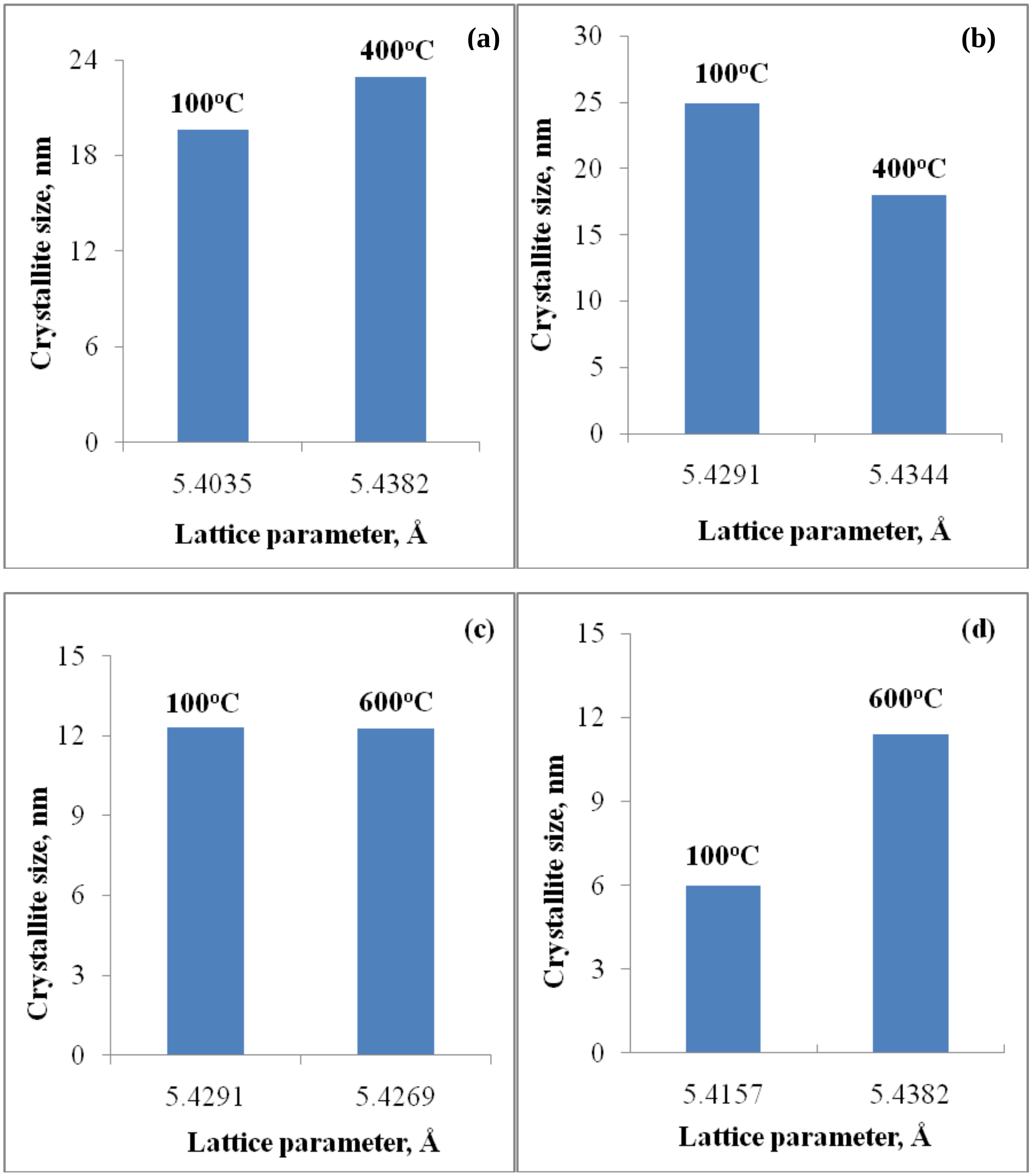

Figure 4.18- Crystallite size as a function of calcination temperatures for nanoplates by H_2O_2 (a), nanocubes (b), nanoplates by NH_4OH (c), and nanorods (d).

By comparing the crystallite size and surface area of ceria nanorods, nanoplates, and nanocubes: nanoplates have high surface area with respect to their crystallite size while nanocubes exhibit high crystallite size at low surface area.

Theoretically, BET specific surface area should increase with the decrease in crystallite size (Tok, 2007). However, this theory only applies to nanorods and nanoplates. In the case of nanocubes, low BET surface area can be accounted for the effect of agglomeration. The agglomerations of these morphologies can be observed in the TEM images described earlier. Table IV-VIII presents the comparison of the surface area with the crystallite size. On the other hand, Figure 4.19 illustrates the concentration of Ce^{3+} as a function of lattice parameter. Higher values of Ce^{3+} ions lead to a larger lattice strain and, consequently, an increase in the lattice parameter of the particles (Deshpande, 2005). Though, in this study, high concentration of Ce^{3+} shows low lattice parameter. This is due to high oxygen vacancies which can induce the lattice parameter to change.

TABLE IV-VIII

BET SPECIFIC SURFACE AREA AND CYRSTALLITE SIZE OF DIFFERENT CeO_2 SHAPES

Precursor	H_2O_2	NH_4OH	NaOH-6M	NaOH-9M
Shape	Nanoplate	Nanoplate	Nanocube	Nanorod
BET surface area (m²/g)	95.11	62.07	16.55	16.74
Crystallite size (nm)	24.92	12.30	19.65	5.97

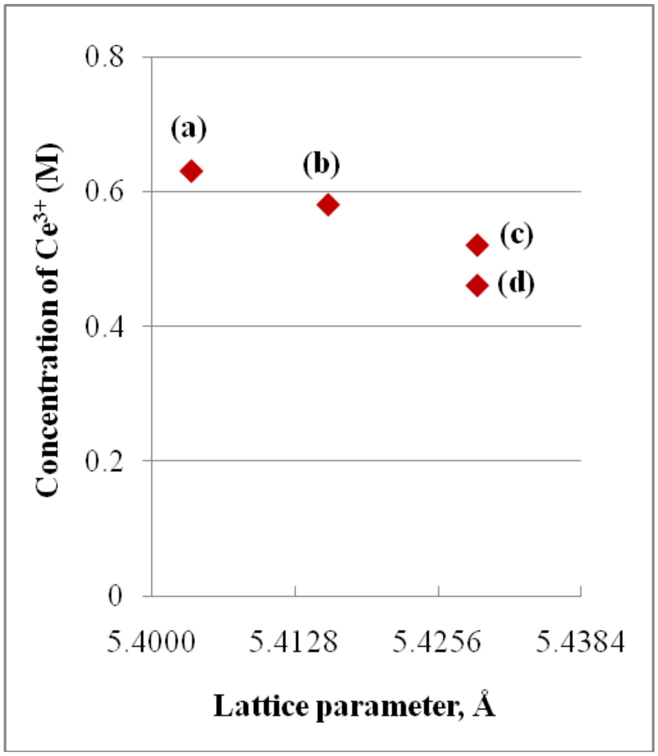

FIGURE 4.19 – Concentration of Ce^{3+} as a function of lattice parameter for CeO_2 nanocubes (a), nanorods (b), nanoplates by NH_4OH (c), and nanoplates by H_2O_2.

In summary, from all the characterizations performed to the synthesized CeO_2 nanomaterials, we can conclude that the precursors and reaction parameters have a significant effect on the morphology of ceria. Nanoplates, nanorods and nanocubes presented different and unique properties. To enhance catalytic performance, CO oxidation is an important process in the three-way catalysis. In order to design and synthesize CeO_2 nanostructured catalyst, decrease in the less reactive crystal planes and increase in the more reactive ones is needed to optimize the desired structure of the active sites. However, it has been a very difficult task for most of the practical catalysts (Kung, 2003). In general, high-surface area nanocatalytic materials exhibiting numerous crystal faces, edges, and corners, which are conventionally considered active sites for the adsorption of reactants (Terribile, 1997; Daturi, 2000 and Stoimenov, 2003), should generate better catalytic performance.

Thus, it is reasonable to consider that the different catalytic properties of various CeO_2 nanomaterials may occur from their morphologies and sizes. The CO oxidation activity of CeO_2 is strongly influenced by the crystal planes due to their different ability of creating oxygen vacancies which are the key point for the CO oxidation. In the present study, the frequently exposed crystal plane in CeO_2 nanoplates, nanorods and nanocubes is (111) plane. The (111) is the most stable surface which has the lowest surface energy (Lundberg, 2004), followed by (110), (100), and (211). Sayle et al. (2002) found that (100) is more reactive and important catalytically as compared with either (110) or the (111) plane. Previous computer modeling demonstrates that less energy is required to form vacancies on (100) than that on (110) and (111). This results suggest that the exposure of more reactive (100) surfaces should facilitate the formation of oxygen vacancies and enhance the OSC (oxygen storage capacity) of CeO_2 (Mai, 2005). Lundberg et al. (2004) found that the more exposure of (100) surfaces in ceria can greatly enhance its CO activity.

This research shows that ceria nanoplates synthesized with H_2O_2 and NH_4OH are mesoporous and have higher surface area than nanocubes and nanorods. Nanorods have compatible surface area as nanocubes synthesized with NaOH, however, they have more exposed crystalline planes (111), (200), and (220) than nanocubes and nanoplates. To provide active sites for catalytic reactions, it is necessary that the exposed planes with higher surface energy could be generated and stabilized (Zhou, 2005). We found that nanorods have also higher concentration of Ce^{3+} than nanoplates which is important for OSC and redox reactions. Nanorods also have smaller crystallite size. The XPS, BET and XRD results in this thesis elucidate that nanorods are better catalyst for CO oxidation and OSC (Mai 2005, Zhou 2005, Tana 2009).

V. CONCLUSIONS

The selection of precursors (H_2O_2, NaOH and NH_4OH) in the synthesis of ceria has yielded different results in terms of crystallite size, crystallinity, particle size, and specific surface area and oxygen vacancy. CeO_2 nanoplates, nanocubes, and nanorods were studied by TEM, BET specific surface area, XPS and XRD. Nanoplates (H_2O_2) and nanorods had a crystallite size range of 22-25nm and 5-11 nm, respectively. The crystallite size was proportional to the calcination temperature and lattice parameter. Nanocubes' crystallite size decreased with the increase of calcination temperature and lattice parameter while nanoplates (NH_4OH) remained constant in the size of 12.3 nm regardless of temperature and lattice parameter. From TEM, agglomeration is observed in nanoplates. Mesoporous material was found in nanoplates by H_2O_2 and NH_4OH, nanorods and nanocubes due to their adsorption-desorption isotherm and pore size distribution. Their pore size was in the range of 7-15 nm according to BJH adsorption model. CeO_2 structures share the same exposing plane (111) and same interplanar d-spacings although their lattice parameters were slightly different from each other. Nanoplates with H_2O_2 have larger particle size than nanoplates with NH_4OH; nanorods have smaller particle size than nanocubes. After the characterization and analysis, nanorods are considered better catalyst for CO oxidation and oxygen storage capacity (OSC).

VI. RECOMMENDATIONS

It was found that high temperature did not affect the crystal structure of ceria nanoplates synthesized using H_2O_2, so it is necessary to conduct synthesis of nanoplates at different concentrations of H_2O_2 and observe any significant differences in size and crystal structure. Ceria nanoplates using NH_4OH need to be studied at higher synthesis temperatures and concentrations of NH_4OH since is uncertain the effect of higher temperature and concentration on the shape and size of nanoplates. For nanorods and nanocubes, decrease the hydrothermal time to see if the crystal size and structure change. Also, it will be helpful if the precipitates are stored longer before characterization and note if time has a significant effect on the crystal structure of ceria.

As mentioned in other studies, other types of characterizations such as particle size analyzer, FT-IR, and TG-DTA will be helpful to better understand the morphology and particle size of ceria nanostructures. Finally, it is necessary to perform CO oxidation to find out the catalytic evaluation and oxygen storage capacity by H_2- TPR in order to understand this behavior. TEM images of ceria nanomaterials after calcination are needed to evaluate their exposing planes.

APPENDIX 1– RAW DATA

TABLE A1 – 1

EXPERIMENTAL DATA FOR CERIA NANOPLATES USING H2O2

Conc. (ml) [0.05M $Ce(NO_3)_3$]	**Conc. 30% H_2O_2 (ml)**	**Color (Before)**	**Temperature (^oC)**	**Time (hr)**	**Color (After)**
8	8	orangish	220	24	white
8	8	orangish	180	24	milky color (white)
8	10	orangish	100	24	white transparent
8	8	orangish	200	3	milky color (white)
8	8	orangish	100	24	white
8	8	orangish	220	24	white
8	8	orangish	220	24	white
8	10	orangish	220	24	white
8	8	orangish	220	24	white
8	8	orangish	250	3	white
8	8	orangish	250	12	white
8	10	orangish	200	24	white
8	8	orangish	220	24	white

TABLE A1 – 2

EXPERIMENTAL DATA FOR CERIA NANOPLATES USING NH4OH

Solution [0.05M $Ce(NO_3)_3$] (ml)	**NH_4OH (ml)**	**Color (Before)**	**Temperature (^oC)**	**Time (hr)**	**Color (After)**
10	10	dark orange	100	24	white
10	10	dark orange	150	24	white
10	10	dark orange	150	24	white
10	10	dark orange	100	24	white
10	10	dark orange	100	24	white

TABLE A1 – 3

EXPERIMENTAL DATA FOR CERIA NANORODS AND NANOCUBES

Weight (g) [0.05M $Ce(NO_3)_3$]	**DI Water (ml)**	**Weight NaOH (g)**	**DI Water (ml)**	**Conc. $Ce(NO_3)_3$ (mol/L)**	**C_{NaOH} (M)**	**Color (Before)**	**T (^oC)**	**Time (hr)**	**Color (After)**
0.8682	5	0.0123	35	0.40	0.01	milky	100	24	white
0.8684	5	12.6389	35	0.40	9.03	milky	100	24	milky
0.8686	5	5.6823	35	0.40	4.06	milky	100	24	purple slurry
0.8684	5	2.4543	35	0.40	1.75	milky	100	24	purple slurry
0.868	5	0.0906	35	0.40	0.06	milky white	100	24	white
0.8688	5	12.5983	35	0.40	9.00	milky	100	24	cloudy
0.868	5	0.0143	35	0.40	0.01	white	100	24	white
0.868	5	8.4255	35	0.40	6.02	milky	100	24	cloudy
0.8683	5	2.8075	35	0.40	2.01	milky	100	24	purple slurry
0.8701	5	12.6852	35	0.40	9.06	milky	100	24	cloudy
0.8686	5	12.6855	35	0.40	9.06	milky	180	24	white
0.8685	5	5.6822	35	0.40	4.06	milky	100	24	white
0.8689	5	8.4586	35	0.40	6.04	milky	180	24	white
0.8686	5	12.6842	35	0.40	9.06	milky	100	24	white

APPENDIX 2 – DECONVOLUTED XPS SPECTRUMS

Peak and integrated area values are presented in Tables IV-III and IV-IV.

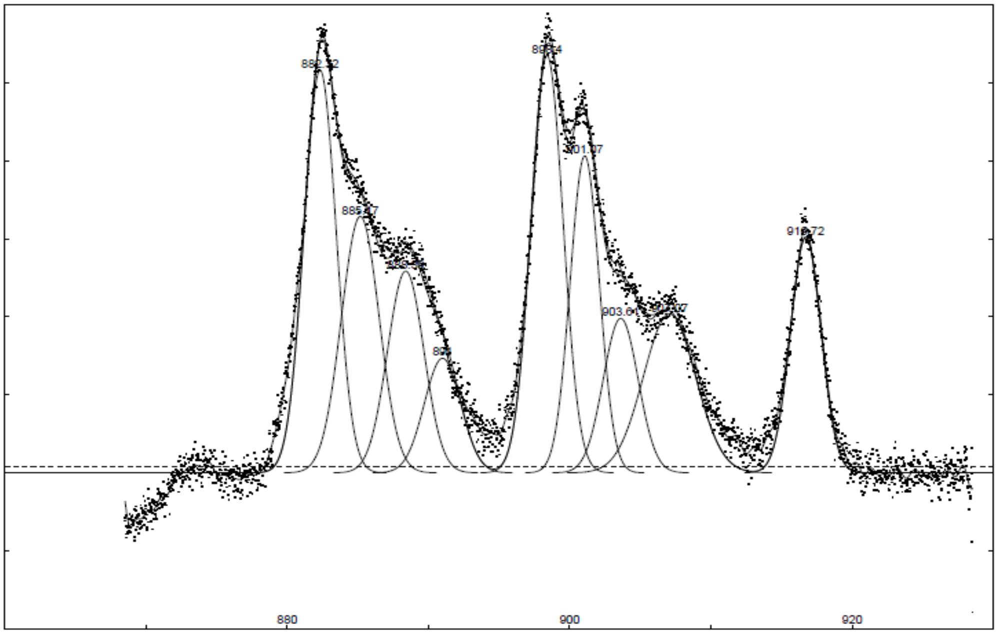

FIGURE A2-1 – CeO_2 nanoplates by H_2O_2 deconvoluted XPS spectrum

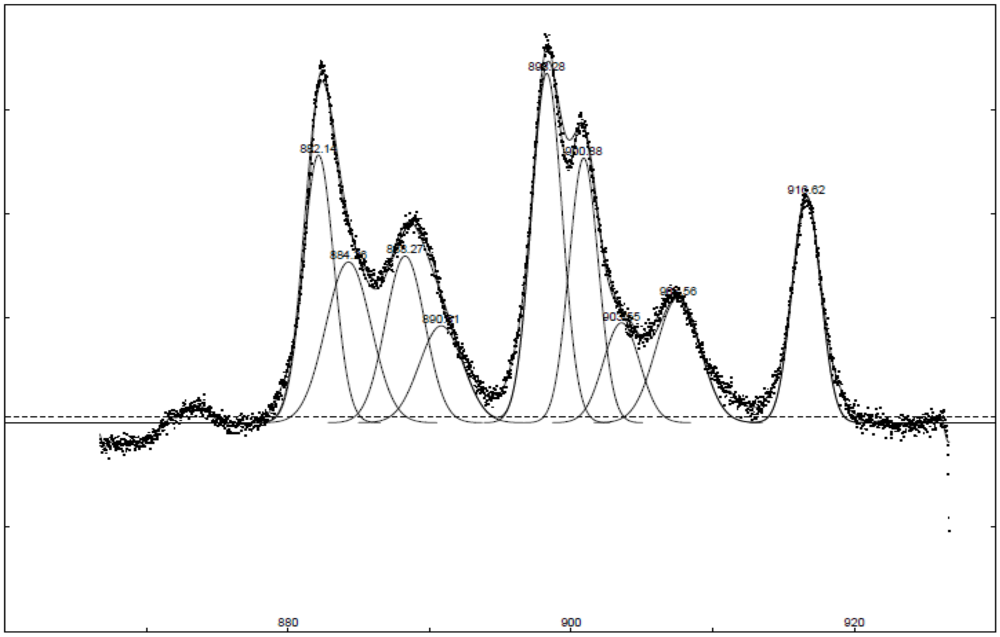

FIGURE A2-2 – CeO_2 nanoplates by NH_4OH deconvoluted XPS spectrum

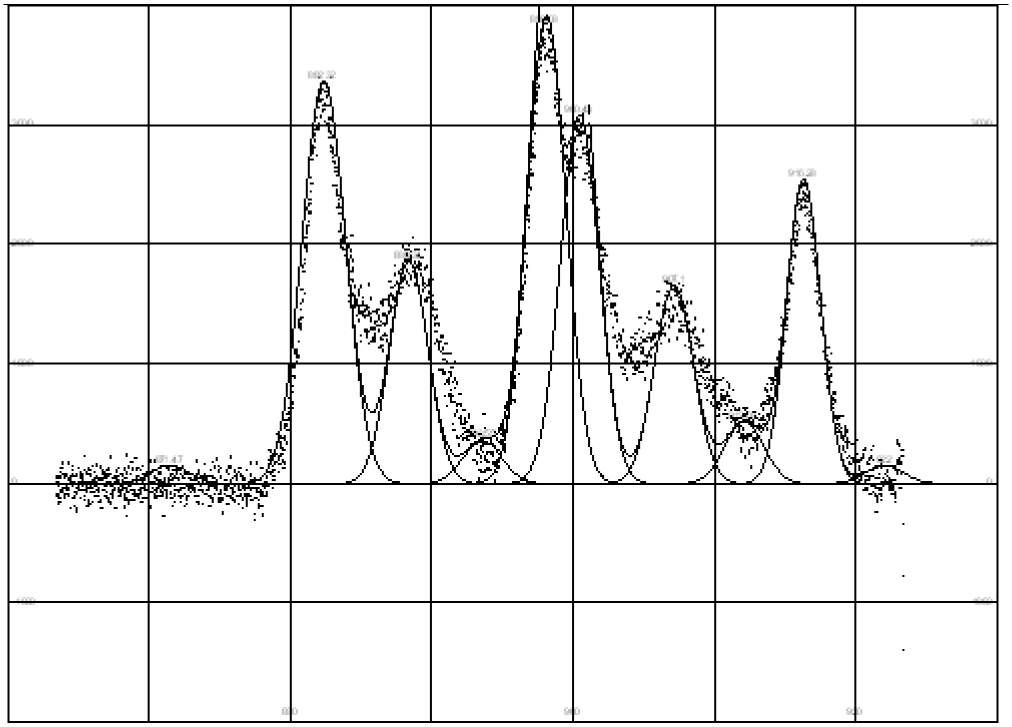

FIGURE A2-3 – CeO_2 nanorods deconvoluted XPS spectrum

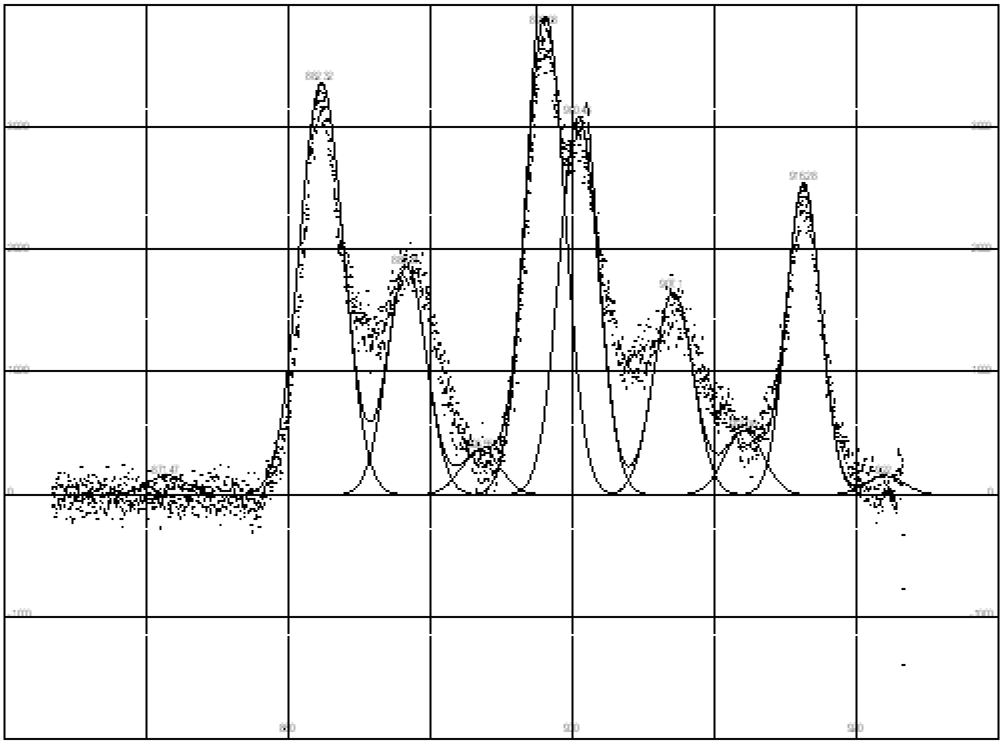

FIGURE A2-4 - CeO_2 nanocubes deconvoluted XPS spectrum

APPENDIX 3: SAMPLE CALCULATION

The following sample calculation is for determining the concentration of Ce^{3+} in a nanoplate. The integrated peak area values are presented in Table IV-IV.

$$[Ce^{3+}] = \frac{14680+11040+10500+9474.21}{14680+11040+8354.20+15220+10500+6139.87+9474.21+8199.964743.22}$$

$$[Ce^{3+}] = 0.52\ M$$

Another sample calculation is for determining the crystallite size and lattice parameter in nanoplates using H_2O_2 at 100^oC. Figure 4.14 will be needed for the calculation

Data Needed

$\lambda = 1.5406$ Å $= 0.15406$ nm	2θ High $= 28.61$
$K = 0.89$	2θ Low $= 28.28$
$(h,k,l) = (111)$	$2\theta_B = 28.45$

Calculate B

$B = (2\theta \text{ High} - 2\theta \text{ Low})*\Pi/180 = (28.61 - 28.28)*\ \Pi/180 = 0.00568$ degree

Calculate θ_B (degree)

$\theta_B = 28.45*\ \Pi/180 = 0.25$ (degree)

Calculate d_{hkl}

$$d_{hkl} = \frac{1.5406}{2 \times \sin 0.25} = 3.31\ \text{Å} = 0.31\ \text{nm}$$

Calculate D_{hkl}

$$D_{hkl} = \frac{0.89x0.15406}{0.00568 \times \cos 0.25} = 24.92\ \text{nm}$$

Calculate *a*

$$a = 3.13 \times \sqrt{1^2 + 1^2 + 1^2} = 5.4291\ \text{Å}$$

REFERENCES

Carrettin, S, Concepción, P, Corma, A, Nieto, J.M, Puntes, V.F. 2004. Nanocrystalline CeO_2 Increases the Activity of Au for CO Oxidation by Two Orders of Magnitude. Angewandte Chemie International Edition 43, 2538.

Chen, H.-I, Chang, H.-Y. 2004. Homogeneous precipitation of cerium dioxide nanoparticles in alcohol/water mixed solvents. Colloids and Surfaces. A: Physicochem. Eng. Aspects 242, 61–69.

Daturi, M,. Finocchio, E, Binet, C., Lavalley, J.-C., Fally, F., Perrichon, V., Vidal, H., Hickey, N., Kašpar, J. 2000. Reduction of High Surface Area CeO_2-ZrO_2 Mixed Oxides. Journal of Physical Chemistry B 104, 9186–9194.

Deshpande, Sameer, Patil, Swanand, VNT Kuchibhatla, Satyanarayana, Seal, Sudipta. 2005. Size Dependendy Variation in Lattice Parameter and Valency States in Nanocrystalline Cerium Oxide. Applied Physics Letters 87, 133113.

Djuricic, B, Pickering, S. 1999. Nanostructured Cerium Oxide: Preparation and Properties of Weakly-agglomerated Powders. Journal of the European Ceramic Society 19, 1925–1934

Gao, Feng, Lu, Qingyi, Komarneni, Sridhar. 2006. Fast synthesis of Cerium Oxide Nanoparticles and Nanorods. Journal of Nanoscience and Nanotechnology 6, 3812-3819.

Groe Johan C., Peffer, Louk A.A., Perez-Ramıırez, Javier. 2003. Pore size determination in modified micro- and mesoporous materials. Pitfalls and limitations in gas adsorption data analysis. Microporous and Mesoporous Materials 60, 1−17.

Han, Wei-Qiang, Wu, Lijun, Zhu, Yimei. 2005. Formation and Oxidation State of CeO2-x Nanotubes**.** Journal American Chemical Soc. 127 (37), 12814- 12815.

Hirano, M, Fukuda, Y, Itawa, H, Hotta, Y, Inagaki, M. 2000. Preparation and Spherical Agglomeration of Crystalline Cerium (IV) Oxide Nanoparticles by Thermal Hydrolysis. Journal of American Ceramic Society 83, 1287-1289.

Kung, Harold H., Kung, Mayfair C. 2003. Heterogeneous catalysis: what lies ahead in nanotechnology. Applied Catalysis 246, 193-196

Lundberg, M., Skårman, B., Wallenberg, L. R. 2004. Crystallography and porosity effects of CO conversion on mesoporous CeO_2. Microporous and Mesoporous Materials 69, 187-195

Mai, H.X, Sun, L.D, Zhang, Y.W., W, Feng, Si, Rui, Zhang, H.P, Liu, H.C., Yan, C.H, 2005. Shape-Selective Synthesis and Oxygen Storage Behavior of Ceria Nanopolyhedra, Nanorods, and Nanocubes. Journal Physics Chemistry, *B* **109,** 24380.

Madier, Y., Descorme, C., Le Govic, A. M., Duprez, D. 1999. Oxygen Mobility in CeO_2 and $Ce_xZr_{(1-x)}O_2$ Compounds: Study by CO Transient Oxidation and $^{18}O/^{16}O$ Isotopic Exchange. Journal of Phyical Chemistry B 103 (50), 10999–11006.

Masui,Toshiyuki, Fujiwara, Kazuyasu, Machida, Ken-ichi, Adachi,Gin-ya. 1997. Characterization of Cerium (IV) Oxide Ultrafine Particles Prepared Using Reversed Micelles. Chemistry of Materials 9, 2197–2204.

Moulder, John F., Stickle, William F., Sobol, Peter E., Bomben, Kenneth D. *Handbook of X-Ray Photoelectron Spectroscopy*, edited by Jil Chastain and Roger C. King Jr. (Physical Electronics, Inc, Minnesota 1995), pp. 142-143.

Pan, Chengsi, Zhanga, Dengsong, Shia, Liyi. 2008. CTAB assisted hydrothermal synthesis, controlled conversion and COoxidation properties of CeO2 nanoplates, nanotubes, and nanorods. Journal of Solid State Chemistry 181, 1298–1306.

Pavasupree, S., Jitputti, J., Ngamsinlapasathian, S., Suzuki, Y., Yoshikawa, Susumu. 2006. Structural, Photocatalytic Activity and Photovoltaic Properties of Mesoporous Anatase Titania Nanopowders Prepared by Hydrothermal Method. Proceedings of the 2nd Joint International Conference on “Sustainable Energy and Environment (Bangkok, Thailand), A-010 (P):1-6

Pavasupree, S., Jitputti, J., Ngamsinlapasathian, S., Suzuki, Y., Yoshikawa, Susumu. 2006. Application of High Surface Area TiO_2 Nanosheet in Dye-sensitized Solar Cells. Proceedings of the 2nd Joint International Conference on “Sustainable Energy and Environment (Bangkok, Thailand), A-008(P): 1-6.

Pavasupreea,S., Suzukia, Y., Pivsa-Artb, Sommai, Yoshikawaa, Susumu. 2005. Synthesis and characterization of nanoporous, nanorods, nanowires metal oxides. Science and Technology of Advanced Materials 6, 224–229

Sayle, D. C., Maicaneanu, S. A., Watson, G. W. 2002. Atomistic Models for CeO_2 (111), (110), and (100) Nanoparticles, Supported on Yttrium-Stabilized Zirconia. Journal of the American Chemical Society 124 (38), 11429–11439

Seal, S, Barr, T. Experimental Methods in the Physical Sciences, edited by H. Singh Nalwa (Academic, New York, 2001), Chap. 2, pp. 111-190.

Si,Rui, Zhang, Ya-Wen, You,Li-Ping, Chun-Hua Yan. 2005. Rare-Earth Oxide Nanopolyhedra, Nanoplates, and Nanodisks. Angewandte Chemie International Edition 44, 3256-3260

Sing, K.S.W, Everett, D. H., Haul, R.A.W., Pierotti, R.A., Rouquerol, J.,Siemieniewska, T. 1985. Reporting Physisorption Data for Gas/Solid Systems with Special Reference to the Determination of Surface Area and Porosity. Pure and Applied Chemistry 57 (4), 603—619.

Sun, C. W., Li, H., Wang, Z. X., Chen, L. Q., Huang, X. 2004. Synthesis and Characterization of Polycrystalline CeO_2 Nanowires. Chemistry Letters 33, 662.

Tana, Zhang, Milin, Li, Juan, Li, Huaju, Li, Yong, Shen, Wenjie.2009. Morphology-dependent redox and catalytic properties of CeO2 nanostructures: Nanowires, nanorods and nanoparticles. Catalysis Today 148, 179–183.

Tang, Bo, Zhuo, Linhai, Ge, Jiechao, Wang, Guangli, Shi, Zhiqiang, Niu, Jinye. 2005. A surfactant-free route to single-crystalline CeO_2 nanowires. Chem. Communications, 3565-3567.

Tarnuzzer, Roy W, Colon, Jimmie, Patil,Swanand, Seal, Sudipta. 2005. Vacandy Engineered Ceria Nanostructures for Protection from Radiation-Induced Cellular Damage. Nano Letters 5, 2573-2577.

Tennyson, Wesley. "X-ray Diffraction: The basics followed by a few examples of data analysis". Internet source, 18 May 2007, available from http://www.nhn.ou.edu/~bumm/NanoLab; accessed 18 May 2007.

Terribile, D., Trovarelli, A., de Leitenburg, C., Dolcetti, G. 1997.Unusual Oxygen Storage/Redox Behavior of High-Surface-Area Ceria Prepared by a Surfactant-Assisted Route. Chemistry of Materials 9, 2676–2678

Tian, Zhengrong R., Voigt, James A., Liu, Jun , McKenzie, Bonnie, McDermott, Matthew J. 2002. Biomimetic Arrays of Oriented Helical ZnO Nanorods and Columns. Journal American Chemical Soc. 124 (44), 12954–12955.

Tok, A.I.Y., Du, S.W., Boey, F.Y.C., Chong, W.K. 2007. Hydrothermal synthesis and characterization of rare earth doped ceria nanoparticles. Materials Science and Engineering A 466, 223–229

Trovarelli, A. 1996. Catalytic Properties of Ceria and CeO_2-Containing Materials. Catalysis. Reviews Science Eng. 38, 439.

Wu, G.S., Xie, T., Yuana, X.Y., Cheng, B.C., Zhang, L.D. 2004. An improved sol–gel template synthetic route to large-scale CeO_2 nanowires. Materials Research Bulletin 39**,** 1023 –1028

Yahiro, H, Baba, Y, Eguchi, K, Arai, H. 1988. High Temperature Fuel Cell with Ceria-Yttria Solid Electrolyte. Journal of the Electrochemical Society 135, 2077- 2080.

Yang, S.W, Gao, L. 2006. Controlled Synthesis and Self-Assembly of CeO_2 Nanocubes. Journal of the American Chemical Society 128 (29), 9330–9331.

Yang, Zhijie, Yang, Yanzhao, Liang, Hui, Liu, Ling. 2009. Hydrothermal synthesis of monodisperse CeO2 nanocubes. Materials Letters 63, 1774–1777.

Zhang ,Ya-Wen, Sun, Xiao, Si, Rui, You, Li-Ping, Yan, Chun-Hua. 2005. Single-Crystalline and Monodisperse LaF_3 Triangular Nanoplates from a Single- Source Precursor. Journal American Chemical Soc. 127 (10), 3260–3261.

Zhou, K.B, Wang, X, Sun, X.M, Peng, Q, Li, Y.D. 2005. Enhanced catalytic activity of ceria nanorods from well-defined reactive crystal planes. Journal of Catalysis 229, 206.

Zhou, X.D, Huebner, W, Anderson, H.U. 2002. Room-temperature homogeneous nucleation synthesis and thermal stability of nanometer single crystal CeO_2. Applied Physics Letters 80 (20), 3814-3816.

Zhou, X.D, Huebner, W, Anderson, H.U. 2003. Processing of Nanometer-Scale CeO_2 Particles. Chemistry of Materials. 15 (2), 378–382.

VITA

NITZIA CHEONG NG

Chemical Engineering Department
J. B. Speed School of Engineering
University of Louisville
Louisville, KY 40292

4103 Blossomwood Dr.
Louisville, KY 40220
n0cheo01@louisville.edu

EDUCATION

Master of Engineering in Chemical Engineering with Environmental Engineering Certificate, University of Louisville, Louisville, KY, 2010

Bachelor of Science in Chemical Engineering, University of Louisville, Louisville, KY, 2009

High School Diploma, Instituto Panamericano, Panama City, Panama, 2003

HONORS AND AWARDS

Awarded international student scholarship from International Center at University of Louisville for Bachelor of Science degree, 2008

Awarded student section award from Society of Women Engineers, University of Louisville, 2009